universität wien

MASTERARBEIT

Titel der Masterarbeit

"Structure and Dynamics of alpha-helical α-Synuclein in a Membrane-Mimetic Environment studied by ^{15}N and ^{13}C NMR-Relaxation"

Verfasserin

Cornelia Haas BBSc

angestrebter akademischer Grad

Master of Science (MSc)

Wien, Februar 2013

Studienkennzahl lt. Studienblatt :	A066863
Studienrichtung lt. Studienblatt:	Biologische Chemie
Betreuer:	Univ. Prof. Dr. Robert Konrat

Abstract

α-Synuclein is being attributed a central role in the etiology of Parkinson disease and other related disorders. Although its function under normal as well as aberrant conditions is still largely a matter of debate, it is expected to involve the transition to an α-helical conformation upon binding a membrane. In the present thesis, α-helical α-Synuclein was studied by NMR spectroscopy in 30% hexafluoroisopropanol (HFIP) as a membrane mimetic solvent. The secondary chemical shift data argues strongly for a continuous helix and against a break which was found in α–Synuclein bound to micelles. The diffusion tensor as well as the $R_2(^{15}N)/R_2(^{13}C)$ relaxation ratio do not disagree with a continuous helical structure, but do not support the hypothesis for a straight helix. The data supports a bent α-helix as was published recently by Braun *et.al* for α–Synuclein in membranes. [1] Other explanations which are supported by the data, could be that the helix is transiently broken, there are oligomeric species present or HFIP forms micro-clusters distorting the tumbling and thereby nuclear relaxation. In order to differentiate between these possible explanations, more experiments would be required.

Zusammenfassung

α-Synuclein hat eine zentrale Rolle in der Entwicklung von Parkinson und anderen artverwandten Krankheiten. Die Funktion unter normalen, sowie aberranten Zuständen ist ein Gegenstand intensiver Diskussion, involviert jedoch einen Übergang zu einer α-helikalen Konformation bei Kontakt mit Membranen. In der hier vorgelegten Masterarbeit, wurde α-helikales α-Synuclein im membranmimetischen Lösungsmittelgemisch 30% Hexafluoroisopropanol (HFIP) mittels NMR-Spektroskopie untersucht. Die Daten der sekundären chemischen Verschiebung unterstützen die Hypothese einer kontinuierlichen Helix. Der Diffusionstensor, sowie das $R_2(^{15}N)/R_2(^{13}C)$ Relaxationsverhältnis sprechen nicht gegen eine kontinuierliche Helix, sie unterstützen jedoch aufgrund des ermittelten Rotationsverhaltens nicht die Hypothese einer geraden Helix. Die Daten passen zu einer gebogenen Helix, ähnlich wie sie vor kurzem von Braun *et.al.* in Membranen nachgewiesen wurde. [1] Andere Erklärungen die mit den vorgelegten Daten möglich wären, sind eine transient gebrochene Helix, oligomere Spezies, oder dass HFIP Micro-cluster formt, welche das Rotationsverhalten beeinflussen. Um zwischen diesen Möglichkeiten zu differenzieren, wären mehr Experimente notwendig.

Acknowledgement

First of all I would like to deeply thank my external supervisors Arthur Palmer III and David Eliezer for their patience to answer my questions and support concerning the practical and theoretical work. I learned a lot!

Secondly I would like to thank my internal supervisor Robert Konrat who generously supported my ambitions and gave me lots of valuable input.

My thank goes also to Jae-Hyun Cho, Michelle Gill and Ying Li for their many hours they spent with me at the spectrometer. Trudy Ramlall was invaluable for me when it came to expressing and purifying the protein. Getting me up and running (somewhat) smoothely on Linux and using the different softwares would not have been possible without the numerously used opportunity to turn around and ask Michelle Gill and Kate Stafford.

Next to mention are Michael and Valentin for their great companionship in finding our ways through life. I hope that we still have a looong way to go.

I also look back in delight to the friends I made in New York aside University, namely Ikuko, Florin, Quing Sudha and Jan.

Contents

1 Introduction

1.1 α-Synuclein

α-Synuclein accumulation and redistribution has a central role in Parkinson disease, dementia with Lewy bodies, pure autonomic failure, and multiple system atrophy. Together these Synucleopathies affect over 5 million people worldwide. [2] Oligomers, protofibrils and fibrils have been detected in diseased human brains. Thereof, the latter are thought to reflect an attempt of the neurons to sequester toxic forms and build them into stable structures with reduced toxicity. The various oligomeric species seem to exist in equilibrium with monomeric α-Synuclein and some of them slowly undergo a transition to fibrils. It is likely that various oligomeric species play a role in the toxicity of α-Synuclein by altering the membrane permeability, damaging mitochondria, triggering lysosomal leakage or disrupting microtubules. [2]

In a healthy nervous system, α-Synuclein is abundantly expressed as it accounts for 1% of total cytosolic protein. [3] In presynaptic terminals it localizes in close proximity, but not within, synaptic vesicles. All three Synucleins (α-, β- and γ-Synuclein) are not essential components of the neurotransmitter release machinery but may contribute to the long-term regulation and maintenance of nerve terminal function. [4] The specific functions are still unclear, except for the following. Burre *et. al.* found that it mediates a nonclassical chaperone activity for the maintenance of continuous presynaptic SNARE-complex assembly. [5]

The α-Synuclein gene encodes for a 140aa protein, which can be divided into a N- and C-terminal domain. The N-terminal domain (aa 1-100) mediates association to membranes and is indispensable for aggregation. It includes 7 imperfect 11-residue repeats, each containing a variant of the consensus sequence KTKEGV, which is similar to the repeats found in class A_2 amphiphatic α-helices, common to apolipo- and other lipid-binding proteins. [6] The C-terminal domain (aa 100-140) has been implicated in regulating its localization and interaction with metals, small molecules and proteins. [2]

The protein does not have a defined structure in aqueous solution. In fibrils a β-rich structure is adopted. Upon interaction with membranes and in oligomers, the N-terminal domain adopts a highly helical structure. In the case of membranes, the N-terminal domain inserts

into the membrane, in an initiation-elongation process. [7] Contrary to common amphiphatic helices, the hydrophobic patch created upon formation of an α-helix in α-Synuclein winds itself around in a right-handed fashion. [8] The C-terminal region remains disordered and does not form direct contacts with the membrane. The interaction with membranes appears to be critical for the normal function in the presynaptic terminals and in aggregation, as shown in figure 1. [6], [9] In micelles, the N-terminal region forms two antiparallel α-helices connected by an extended linker of 4-6 residues around V40. [10], [11], [12] Increasing the size of the micelle to which the protein was bound, lead to the two helices splaying further apart. [13] In vesicles and bicelles the two helices fuse and form a single extended helix, as was shown by electron spin resonance (ESR) in combination with computer modelling and single-molecule Förster resonance energy transfer (FRET). [14], [15], [16]

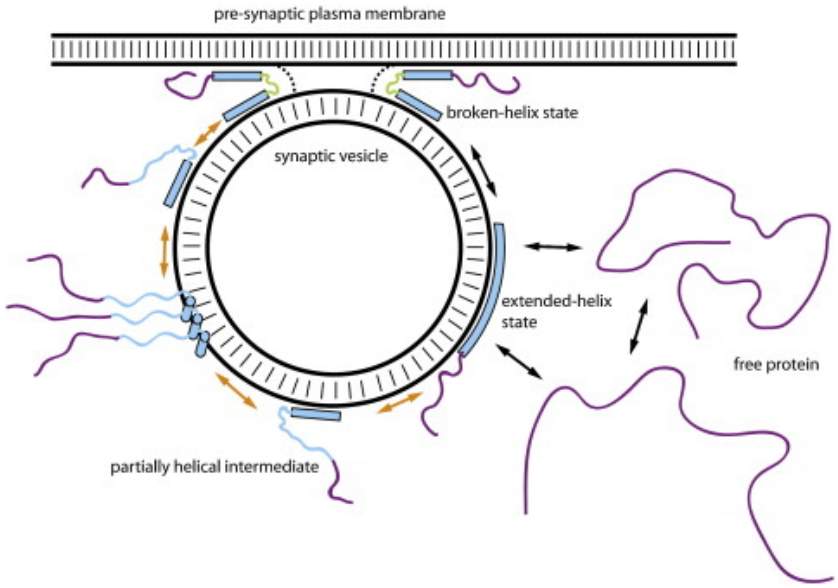

Figure 1 – Models for the membrane-induced structure, function and aggregation of α-Synuclein. The free, unstructured state (solid line) is in equilibrium with vesicle-bound states. The helical regions (filled bars) may be broken or extended on the vesicle. Upon approaching another membrane, the two helices of the broken helical state may insert into different bilayers. Taken from [6]

1.2 Aim and Experimental Approach

In order to gain insight into the molecular detail of the extended state of α-Synuclein, which is not possible with the methods which were used to detect the extended state, a different methodology had to be chosen. X-ray crystallography, NMR and to a limited extent molecular dynamics (MD) are the only methods which are able to provide this level of detail, as

depicted in figure 2. Due to difficulties obtaining crystals for membrane-proteins in general and specifically for the case of only one or two membrane-embedded helices, X-ray crystallography is here not a very promising method. MD is well able to provide the desired level of detail, but would need support from experimental methods in this case. In fact, the only two published membrane-associated structures 1XQ8 and 2KKW were studied by NMR spectroscopy in combination with electron pulse resonance (EPR). [11], [12] In both cases, micelle-bound α-Synuclein was in the broken helix state.

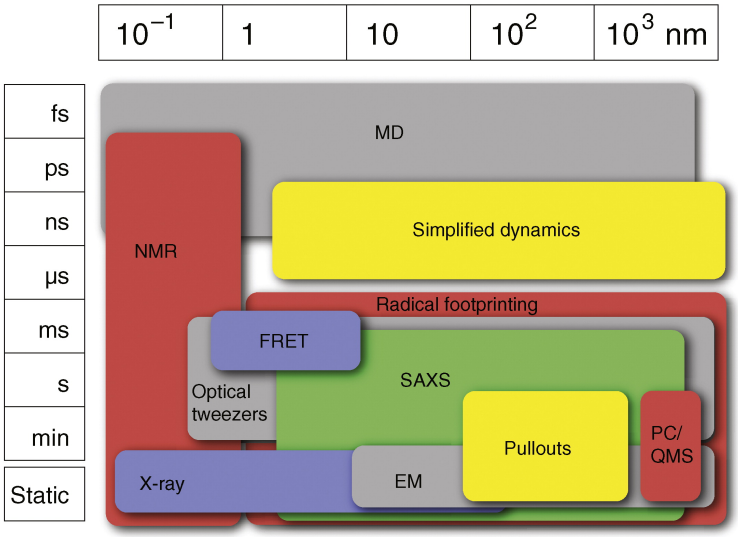

Figure 2 – An overview of the spatial and temporal coverage of various methods. The x-axis represents the size of the systems that can be explored by each method in nanometers. The y-axis represents the time scales that can be reached. SAXS (small angle X-ray scattering), PC/QMS (pulse-chase monitored by quantitative mass spectrometry), FRET (Förster resonance energy transfer), MD (Molecular dynamics). Taken from [17]

Upon increasing the size from SDS-micelles (5 nm diameter) towards synaptic vesicles (10x larger) to attain the extended helical state, the diffusion slows down and therefore transverse relaxation of nuclear spin magnetization gets faster, precluding multidimensional NMR-experiments. Bodner *et. al.* probed this "dark state" by transferred NOEs ($H^N \rightarrow H^N$ and Leu-$C^{\delta 1}H_3 \rightarrow H^N$) and confirmed an α-helical conformation of a 'segment of residues' starting at the N-terminus, whereas the 40 C-terminal residues remain dynamically disordered. [18]

Membrane mimetic solvents, such as trifluoroethanol (TFE) or hexafluoroisopropanol (HFIP) may bridge this gap in that they facilitate a hydrophobic/hydrophilic environment to support helix-formation as well as rapid diffusion to slow down transverse relaxation.

1.2.1 Membrane mimetic solvents

Fluorinated alcohols, such as TFE or HFIP are known for their structure stabilizing properties and have been used as membrane mimetic environments in several NMR-studies. [19], [20], [21] The chemical shifts were found to be only slightly changed, although their temperature sensitivity is altered. [22] The largest effect on proteins for both alcohols was found to be in an aqueous solution with 30% cosolvent. [23] Despite the large amount of experimental data accumulated in the last decades, the mechanism by which these cosolvents stabilize proteins or peptides remains a matter of debate. It is postulated that it is mediated by a reinforcement of hydrogen bonds between carbonyl and amide N-H groups by the removal of water molecules in the proximity of the solute and/or lowering of the dielectric constant of the medium. [24] Furthermore, the low polarity of the cosolvent allows formation of micro-clusters in aqueous solution. This provides a solvent matrix which promotes hydrophobic interactions between amino acid side chains. The microclusters may potentially also coat the peptide surface and reduce its interaction with water, and thus stabilizes the helical conformation. HFIP has in comparison to TFE a slightly stronger secondary structure stabilizing effect and was therefore used in the experiments.

Before investigating the intramolecular dynamics of the extended state, the existence of this structure in HFIP has to be proven and was the scope of this thesis. Three NMR-approaches were chosen to answer this question:

1.2.2 Secondary Chemical Shifts

Chemical shifts are strongly dependent on the protein secondary structure and have been used extensively for more than two decades to get information on the identity, extent and location of secondary structural elements. [25] Therefore a set of amino acid-dependent random coil shifts are subtracted from the measured chemical shifts and the sign and size of this secondary chemical shift is evaluated. In the case of $^{13}C_\alpha$, the nucleus which generally gives the best results, stretches with positive chemical shift values correlate with α-helices and negative stretches with β-sheets. The magnitude of the chemical shifts gives information about the propensity of the structural element. Values around zero, correspond to unstructured regions. Also other nuclei, such as ^{15}N, $^{1}H_N$,$^{1}H_\alpha$, $^{13}C_\beta$ and ^{13}CO have been used successfully for

chemical shift indexing, although their chemical shifts tend to be more sensitive towards other structural features than the chemical shifts of α-carbons [26] , [27].

1.2.3 Diffusion Tensor

The global shape of a molecule has a profound effect on the physics of spin relaxation because the spectral density function depends on the relative orientation of the axis system of the relaxation mechanisms and the diffusion tensor. Thereby, it is a prerequisite to have a valid diffusion-model in order to describe internal motion, e.g. in a Lipari-Szabo type analysis.

In the following section, the necessary terminology will be explained:

Relaxation Relaxation is the return of a system to equilibrium and is characterised by rate constants. The magnitudes of the rate constants are governed by $\langle \delta\omega^2 \rangle \tau_c$. [28] Therein, the correlation time τ_c, describes the stochastic motion of the spin in the molecule. $\langle \delta\omega^2 \rangle$ is the mean square variation in the local magnetic field of the active Hamiltonian. The motional process of interest defines the correlation time and sets the quest for finding a Hamiltonian exhibiting a large variance at the timescale of interest. For nano-picosecond motion of spin 1/2 nuclei, chemical shift anisotropy (CSA) and dipole-dipole interactions (DD) exhibit the largest variances, and are therefore efficient relaxation mechanism.

Relaxation Mechanisms Dipole-dipole interaction (DD): Any nucleus with a nonzero spin angular momentum generates a magnetic field. Depending on the molecular orientation during tumbling in solution, this magnetic dipolar field adds to or subtracts to the fields experienced by other nuclei in proximity. This dipole-dipole interaction depends quadratically on the magnetogyric ratios γ_I and γ_S for the nuclei I and S as well as the internuclear distance to the sixth power. The dipolar relaxation is highest among protons due to their high magnetogyric ratio and a single proton can exhibit this interaction with several others. For heteronuclei only the dipolar interaction with the attached proton is close enough to have a relevant effect, thereby simplifying data interpretation and making the heteronuclei an ideal system to study relaxation. $\mu_0$is the permeability of vacuum, $\hbar$ is Planck's constant.

$c_{DD}^2 = \frac{\left(\frac{\mu_0}{4\pi}\right)^2 \hbar^2 \gamma_I^2 \gamma_S^2}{r_{IS}^6}$

Chemical shift anisotropy (CSA): Chemical shifts are reflections of the electronic environments that modify the local magnetic fields. As chemical shifts are anisotropic, the field

experienced by this nucleus fluctuates depending on the orientation of the nucleus to the external field. The magnitude of this variance depends quadratically on the intrinsic chemical shift anisotropy $\Delta\sigma$ (assuming a cylindrically symmetric chemical shift tensor) and also quadratically on the magnetic field strenght B_0. The first term is on the order of the chemical shift range of the respective nucleus, making it more important for nuclei with large chemical shift ranges, such as carbon, nitrogen and phosphorous.

$$c^2_{CSA} = \Delta\sigma\gamma_I B_0/\sqrt{3}$$

The relative contributions of the two mechanisms depend on the spin system, but together they entail relaxation time constants on the order of milliseconds to seconds. In the case of ^{15}N bonded to one proton the ratio of the CSA- to DD-constants increases from 0.67 for 500 MHz to 1.5 for 750 Mhz. For monoprotonated ^{13}C the ratio is even at 750 MHz only 0.05, thus sole consideration of the DD mechanism is a well justified approximation for ^{13}C relaxation studies, but not for ^{15}N data interpretation. [29]

Describing Motion: Spectral Density Function The rotational correlation time τ_c can be understood as the average time a spin requires to move by one radian. For an approximately spherical globular protein, the correlation time is related to its effective hydrodynamic radius (a) according to the Stokes-Einstein equation. Therein, η is the dynamic viscosity, k is the Boltzmann constant and T is the temperature.

$$\tau_c \approx \frac{4\pi\eta a^3}{3kT}$$

The correlation time also exhibits a good empirical correlation with the molecular weight, as seen in figure 3. [30]

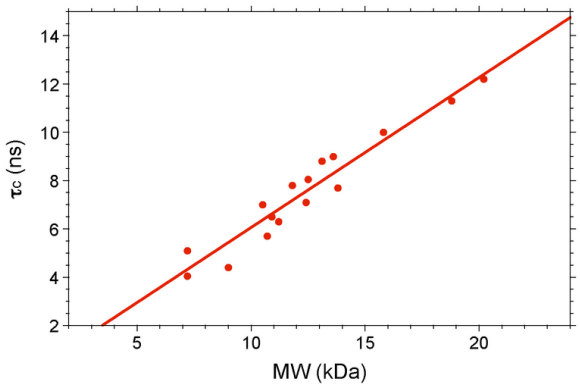

Figure 3 – Rotational correlation times and molecular weights for sixteen monomeric proteins. The correlation times were determined by ^{15}N relaxation measurement. Taken from [30]

Mathematically, the rotational diffusion is described by a correlation funtion C(τ) which is a simple exponential whose decay rate is set by τ_c, if the molecule is assumed to be spherical and the solvent simply provides a medium with a certain viscosity. The Fourier Transform of the correlation function gives the spectral density J(ω). The spectral density gives information about the extent of motion at different motional frequencies as seen in figure 4.

$C(\tau) \overset{FT}{\leftrightarrow} J(\omega) = \frac{\tau_c}{1+\omega^2\tau_c^2}$

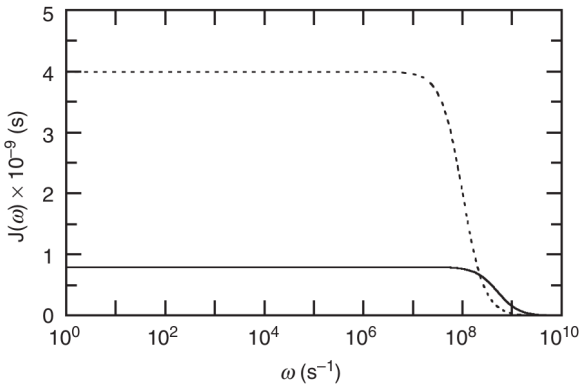

Figure 4 – Spectral density functions for an isotropically diffusing molecule with (—) τ_c= 2 ns and (···)τ_c= 10 ns. Taken from [28]

In the case of anisotropic diffusion, the correlation function and spectral density need to account for the rotational anisotropy by incorporating the three principal values D_{xx}, D_{yy}, D_{zz} of the diffusion tensor **D**: [31]

$J(\omega) = \sum_{j=1}^{5} A_{ji} \frac{\tau_j}{1+\omega^2\tau_j^2}$

where:

$\tau_1 = (4D_{xx} + D_{yy} + D_{zz})^{-1}$

$\tau_2 = (D_{xx} + 4D_{yy} + D_{zz})^{-1}$

$\tau_3 = (D_{xx} + D_{yy} + 4D_{zz})^{-1}$

$\tau_4 = (6D_{iso} + 6\sqrt{D_{iso}^2 - \frac{D_{xx}D_{yy}+D_{xx}D_{zz}+D_{yy}D_{zz}}{3}})^{-1}$

$\tau_5 = (6D_{iso} - 6\sqrt{D_{iso}^2 - \frac{D_{xx}D_{yy}+D_{xx}D_{zz}+D_{yy}D_{zz}}{3}})^{-1}$

$A_{1i} = 3y_i^2 z_i^2$

$A_{2i} = 3x_i^2 z_i^2$

$A_{3i} = 3x_i^2 y_i^2$

$A_{4i} = 1/4[3(x_i^4+y_i^4+z_i^4)-1]-1/12[\delta_x(3x_i^4+6y_i^2z_i^2-1)+\delta_y(3y_i^4+6x_i^2z_i^2-1)+\delta_z(3z_i^4+6x_i^2y_i^2-1)]$

$A_{5i} = 1/4[3(x_i^4+y_i^4+z_i^4)-1]+1/12[\delta_x(3x_i^4+6y_i^2z_i^2-1)+\delta_y(3y_i^4+6x_i^2z_i^2-1)+\delta_z(3z_i^4+6x_i^2y_i^2-1)]$

$D_{iso} = \frac{Trace\{\mathbf{D}\}}{3} = \frac{D_{xx}+D_{yy}+D_{zz}}{3}$

$\delta_k = \sqrt{\frac{D_{kk}-D_{iso}}{D_{iso}^2 - \frac{D_{xx}D_{yy}+D_{xx}D_{zz}+D_{yy}D_{zz}}{3}}}$ for k=x, y, z

$\mathbf{e}_i = (x_i, y_i, z_i)$ are the direction cosines defining the orientation of the ithX-H bond vector in the principal axis frame of the diffusion tensor

For an axially symmetric diffusing molecule, the Diffusion tensor **D** has only two components $D_\perp = D_{xx}=D_{yy}$ and $D_\parallel=D_{zz}$ and the equations are somewhat simlified.

Relaxation rates For each spin operator the relaxation rates are the sums of spectral density values J(ω) sampled at certain frequencies multiplied by the constants, specific to the relaxation mechanism (c_{DD} and c_{CSA}). There are five sampling frequencies for the spectral density ω_0, ω_I, ω_S, (ω_I-ω_S) and (ω_I+ω_S).

The longitudinal $R(S_z)$ and the transverse $R(S_x)$ relaxation rates of heteronuclear atoms are the most frequently studied operators when investigating protein dynamics. Their equations are given below [32]:

$R(S_z) = R_1 \propto J(\omega_S)(3c_{DD}^2 + c_{CSA}^2) + J(\omega_I - \omega_S)c_{DD}^2 + J(\omega_I + \omega_S)6c_{DD}^2$

$R(S_x) = R_2 \propto J(\omega_0)(2c_{DD}^2 + 2/3c_{CSA}^2) + J(\omega_S)(3/2c_{DD}^2 + 1/2c_{CSA}^2) + J(\omega_I)3c_{DD}^2 + J(\omega_I - \omega_S)1/2c_{DD}^2 + J(\omega_I + \omega_S)3c_{DD}^2$

Diffusion tensor The diffusion tensor may be calculated by fitting the experimental R_2/R_1 relaxation data to the components of the diffusion tensor. [33] In the case of isotropic diffusion the only component is τ_c. A full description of the asymmetric diffusion tensors requires the amplitude and orientation of the principle components of the diffusion tensor. In the case of the axially symmetric diffusion tensor these are $D_\perp$, $D_\parallel$ and two angles. The fully asymmetric diffusion tensor is described by 6 components (D_{xx}, D_{yy} , $D_{zz}$and three angles). During an analysis, the parameters of the different diffusion tensor models are optimized and need to be evaluated by statistical analysis in order to test for their ability to reproduce the measured relaxation rates. Depending on the model which is accepted, information on the overall geometry of the molecule, and therefore evidence for or against the extended α-helix in α-Synuclein may be obtained.

In most cases ^{15}N relaxation data is used to calculate the diffusion tensor. However, due to the limited sampling of space in the case of ^{15}N relaxation data for an extended helix which will be discussed below, it is important to incorporate also $^{13}C_\alpha$ relaxation data. [34]

1.2.4 Relaxation and rotational anisotropy

A single straight helix resembles a rod, which is expected to turn much faster around the cylindrical axis than tilt. In the helix, the backbone N-H and C_α-H bond vectors point in orthogonal directions, as shown in figure 5. As the turning is much faster than the tilting of a helix, the C_α-H bond vectors experience much faster motion than the N-H bond vectors. Faster motion correspond to a spectral density function which extends to higher frequencies and has a reduced amplitude (see fig. 4). This reduced amplitude leads to slower R_2 relaxation in the case of macromolecules. Therefore, a single straight helix is expected to exhibit a higher nitrogen relaxation rate compared to the α-carbon relaxation rate, when accounting for nucleus-specific factors.

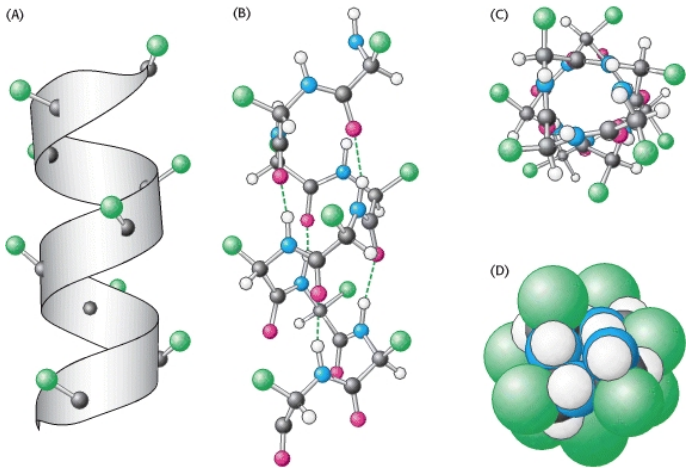

Figure 5 – α-Helix (a) Ribbon depiction with the α-carbon atoms (black) and side chains (green) shown. (b) Side view of a ball-and-stick version depicts the hydrogen bonds (dashed lines) between NH and CO groups pointing along the helix. (c) End view shows the coiled backbone as the inside of the helix and the C_α-hydrogens (white) and side chains projecting outward. (d) Space-filling view of part C. Taken from [35]

1.2.5 Isotopic Labeling

In order to surmount one bond ^{13}C-^{13}C coupling, isotopic enrichment at alternating carbon sites was used. This can be done by expressing the protein in a medium containing 2-^{13}C glycerol. When using an *E. coli* strain in which the citrate cycle was modified, LeMaster *et. al.* got a labeling pattern in which most α-carbon sites are labeled (90+%) and the β-carbons are not (1%) as seen in figure 6a. [36] Exceptions are Ile and Val, where also the β-carbon is labelled and Arg, Glu/Gln, Leu and Pro where the opposite alternate labeling was found. Using a modern *E. coli* strain for protein expression, the labeling pattern is somewhat

less clear. [37] In this case, Arg, Glu/Gln, Leu and Pro are not labelled beyond 30% at the α-carbon sites, but also Asp/Asn, Ile and Thr only exhibit a fractional labeling (40-80%). The labeling at the β-position was not measured, but may be assumed to be reciprocal to the labelling at the α-position, except for Ile and Val.

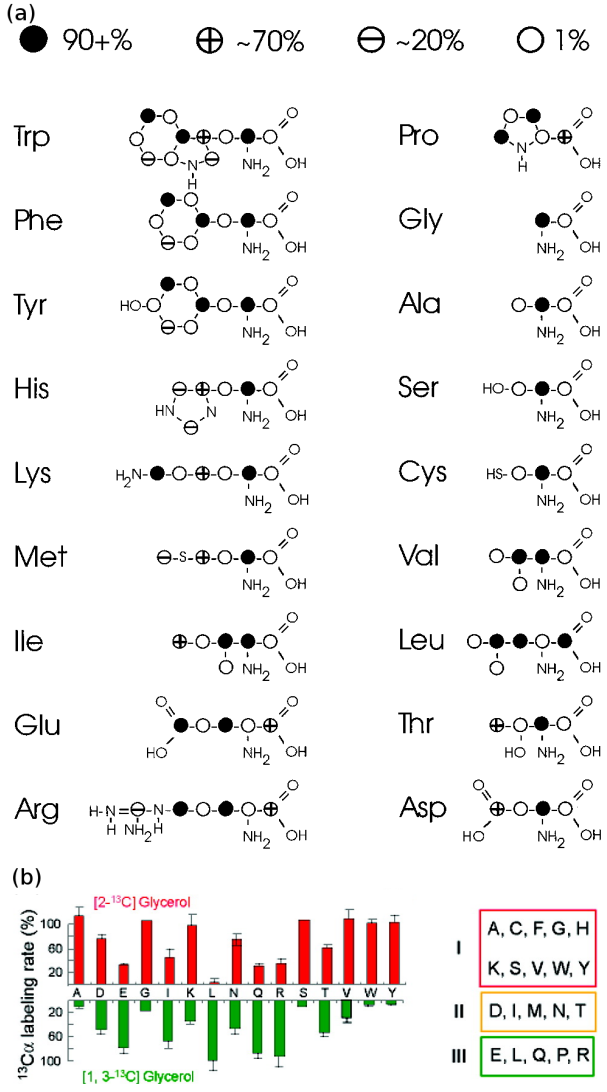

Figure 6 – Labeling pattern of 2-^{13}C glycerol. (a) Metabolic labeling achieved when interrupting the citrate cycle in *E. coli*. Taken from [36] (b) Metabolic labeling using a conventional *E. coli* -strain for protein expression. Taken from [37]

In the studied truncated version of α-Synuclein, there are no Arg, eight Asp (E13, E20, E28, E35, E46, E57, E61, E83), four Asn (Q24, Q62, Q79, Q99), three Leu (L8, L38, L100) and no Pro and a significant proportion of them only gives very low S/N in ^{13}C-spectra. There is one Ile (I88), but there are 18 Val (V3, V15, V16, V26, V37, V40, V48, V49, V52, V55, V63, V66, V70, V71, V74, V77, V82 and V95).

2 Materials and Methods

2.1 Protein Production

2.1.1 Expression and Labelling

The α-Synuclein gene was on a plasmid construct kindly provided by Dr Peter Lansbury (Dept. of Neurology, Harvard Medical School) in which the α-Synuclein gene is under the control of a strong phage T7 promoter. As only the N-terminal domain adopts an α-helical conformation, a truncated version of α-Synuclein was used in all experiments (amino acids 1–102). The truncation was done by insterting two stop codons after K102 using the Stratagene QuickChange ^{TM}Site-directed Mutagenesis Kit to avoid leaky expression. The truncation was confirmed by sequencing. The protein was expressed in *Escherichia coli* BL21 DE3 (Novagen) grown in 4 l minimal medium (for composition see 2.1.3), spun down (10,000 g) at an OD_{600} of approx. 0.7 and then resuspended in 1 l of fresh isotopically labelled minimal medium. Therein, the expression was induced using 0.8 mM IPTG (isopropylthiogalactoside) and the cells grown for 3.5 hours. The cells were spun down again and the pellet frozen at -20°C until purification.

2.1.2 Purification

The purification followed a previously published protocol [38] and [39], with some modifications. All steps until the HPLC were done on ice or at 4^oC. The cell pellet was resuspended in 50 ml lysis buffer and sonicated for 10 min. to break up the cells. The soluble fraction was separated from the cell debris by ultracentrifugation (180.000 g for 1h) and any remaining DNA precipitated by addition of 1% w/v streptomycin and subsequent centrifugation (27,000 g). Afterwards, some cellular proteins were precipitated and removed by centrifugation (27,000 g) in 12% w/v ammonium sulfate. α-Synuclein was precipitated and spun down (27,000 g) by addition of another 13% w/v ammonium sulfate. The pellet was resuspended in 50 ml lysis buffer (without DTT) and dialysed over night into the low-salt ion exchange loading buffer. Using the FPLC-system ÄKTApurifier^{TM}, the sample was loaded onto a cation exchange column (HiPrep 16/10 CM FF, GE Healthcare Life Sciences) and eluted by a high-salt elution buffer. The fractions containing α-Synuclein were identified by gel electrophoresis, pooled and dialysed over night into 5% acetic acid. After dialysis, the sample was injected onto the C4 re-

verse column (VYDAC) on the Waters 2690 Separations HPLC system and rinsed with HPLC loading buffer. The protein was eluted by hydrophobic replacement with acetonitrile in the HPLC elution buffer. The protein-containing fractions were identified by UV_{229} absorbance and collected separately. Trifluoroacetic acid from the HPLC buffers was removed by application of the pooled fractions onto VariPure^{TM}IPE gravity-flow columns (Agilent Technologies). Acetonitrile was removed by centrifugation under vacuum, and water by lyophilization to get pure α-Synuclein.

2.1.3 Media Composition and Chemicals

Lysis Buffer

1 mM EDTA

1 mM DTT

10 mM Tris pH 8.0

1 mM PMSF (phenylmethylsulfonyl fluoride)

3% v/v Protease Inhibitor Cocktail (Sigma-Aldrich)

Minimal Medium

2 g/l Glycerol (unlabelled or 2-^{13}C glycerol (Cambridge Isotopes))

1 g/l Ammonium chloride (unlabelled or ^{15}N-ammonium chloride)

1% v/v vitamin cocktail (Sigma-BME vitamins)

1 mM $MgSO_4$

100 μM $CaCl_2$

6.8 g/l Na_2HPO_4

3 g/l KH_2PO_4

0.5 g/l NaCl

Cation Exchange Loading Buffer

20 mM NaCl

25 mM Tris pH 8.0

1 mM EDTA

Cation Exchange Elution Buffer

1 M NaCl

25 mM Tris pH 8.0

1 mM EDTA

HPLC Loading Buffer

0.1% trifluoroacetic acid

HPLC Elution Buffer

90% acetonitrile

0.1% trifluoroacetic acid

2.2 NMR Instrumentation and Experiments

2.2.1 NMR-Sample preparation

NMR samples were prepared by dissolving 1.5 mg of lyophilized protein in 400 μl D13-MES (D13 2-(N-morpholino)ethanesulfonic acid (Cambridge Isotopes), 50mM, pH 6.0) and spinning down any aggregates at 15.000 rpm for 10 minutes at room temperature. The concentration was determined by UV-absorption at 280 nm (ε = 1490 $cm^{-1}M^{-1}$) and the solution diluted in buffer. DSS (3-(Trimethylsilyl)propane-1-sulfonic acid) and D_2O were added to a final concentration of 50 μM and 5%. Using a Hamilton syringe and working in the cold room with chilled HFIP to reduce evaporation losses, 180 μl D2-HFIP (D2 Hexafluoro-2-propanol (Cambridge Isotopes)) were added. From this procedure 600 μl of 200 μM α-Synuclein in 32 mM D13-MES and 30% D2-HFIP were obtained. The solution was spun down again for 10 min. at 15.000 g in the cold room and transferred into a conventional NMR-tube by a Hamilton syringe and the tube sealed by a Shigemi-plunger. The NMR samples were stored at room temperature between the experiments. The pH of the samples was determined after the NMR experiments and was in the range of pH 6.0 $\pm$ 0.2 pH units.

Sample temperature was calibrated to 323.5 K before every experiment using D6 ethylene glycol (Cambridge isotopes) as previously described. [40]

2.2.2 HNCA Experiments: $^{13}C_{\alpha}$ assignment and secondary shift

The HNCA spectra were taken on a 14.3 T Bruker Avance spectrometer equipped with triple resonance z-axis gradient cryoprobe using a ^{13}C and ^{15}N labelled sample. They were recorded using 1024 x 70 x 54 time points in the ^{1}H x ^{15}N x^{13}C dimension. The offset was set at 4.7 x 115 x 54 ppm and the spectral width was 11.9 x 25 x 30 ppm. For each time point 48 scans were summed up. The exact water frequency differed slightly between the experiments.

The spectra were processed in NMRpipe and Sparky. [41], [42] The free induction decays in the hydrogen dimension was multiplied by a Lorentz-to-Gaus window. In the nitrogen and carbon dimensions the data points were double by a linear prediction of order 16 and multiplied by an optimized Kaiser window. All dimensions were zero-filled to double the data points, fourier transformed and phase shifted to give in-phase spectra.

2.2.3 ^{15}N R_1 and R_2 Hahn Echo Relaxation Experiments

Spectra were taken from a uniformly ^{15}N labelled sample at 11.7, and on a $^{13}C_{\alpha}$ and ^{15}N labelled sample at 18.8 T (Bruker Avance spectrometer equipped with triple resonance z-axis gradient cryoprobe). For the R_1 experiment, 1024 x 256 time points were recorded in the direct / indirect dimension and 32 scans summed up for each of them. The spectral width was 11 ppm x 25 ppm. The relaxation delays were 112.5, 318, 584 and 900 ms, to give a good signal decay. Coupling to H_N during the relaxation delay was refocused by a centered hard 180° pulse on hydrogen.

The R_2 Hahn Echo was recorded with 48 scans per time point and 2048 x 512 time points in the direct / indirect dimension. The spectral width was 11 x 25 ppm. The short and long relaxation delays were 0.176 and 38.688 ms. Coupling to H_N during the relaxation delay was refocused by a WALTZ-16 pulse train.

The R_2 CPMG experiment was recorded with the same spectral parameters as the Hahn Echo, except for the relaxation delays (4, 12, 24 and 40 ms) and the hard pulses every second τ_{cp}used for hydrogen decoupling during the relaxation delay.

Spectral processing was carried out using NMRPipe and Sparky. [41], [42] The free induction decays in both dimensions were multiplied by a cosine function, zero filled to double the number of points, fourier transformed and phase shifted to give in-phase spectra. In the case of the R_2 data, a forward-backward linear prediction with an order of 16 was used to double

the data points. Errorpropagation was done according to the formula proposed by NIST. [43]

Diffusion tensor calculations were done in TENSOR2 [44], using the measured relaxation data and the following structures: a straight helix created in Pymol [45] and 1XQ8 and 2KKW from the PDB database [46].

From the rotational correlation time, the apparent molecular weight was calculated from published data for 16 monomeric spherical molecules. [30] However, this empirical correlation was measured in water at 25°C. To date no relaxation rates or correlation times of proteins in 30% HFIP have been published. When estimating an effective hydrodynamic radius through the Stokes-Einstein equation, both experimental differences were accounted for.[28] Therein, the kinematic viscosity (ν(T)) of pure HFIP at T=50°C was extrapolated by the Arrhenius equation from published data at 25 and 38°C [47], [48], transformed into the dynamic viscosity μ_{HFIP} by multiplying with the density and the dynamic viscosity of the HFIP-water mixture μ_{mix} estimated by the Grunberg equation.

Arrhenius equation: $\nu(T) = \nu_0 \exp(\frac{E}{RT})$

Grunberg equation: $\ln(\mu_{mix}) = X_{HFIP}\ln(\mu_{HFIP}) + X_{H_2O}\ln(\mu_{H_2O})$

ν(T) is the kinematic viscosity at the temperature T, ν_0 is a coefficient, E is the activation energy and R is the universal gas constant, μ is the dynamic viscosity, X is the molar fraction of HFIP, water, and the mixture, respectively

2.2.4 ^{13}C R_2Hahn Echo Relaxation Experiment

Measuring the relaxation rate of $^{13}C_\alpha$ turned out to be more complicated, as the ^{13}C-HSQC was too overlapped to give reliable relaxation rates (see figure 11).

To get resonance dispersion, a HNCA pulse sequence was modified according to the 'reduced dimensionality' principle first introduced by the Wűthrich laboratory [49]. Therefore, the carbon and nitrogen indirect evolution periods were incremented simultaneously rather than independently. This yielded a 2-D spectrum with the H_{N_i} shift on one axis and the summed shifts of C_i+N_i and C_{i-1}+N_i on the second axis. By varying the ratio of the incremented time in both indirect dimensions, the relative contribution of nitrogen versus carbon could be modified. The overall spectral width was modified by increasing or decreasing the incremented times, keeping the relative sizes of the carbon and nitrogen increments constant. The peak distribution of several spectra was computed and verified experimentally to give a

spectrum with a good signal dispersion as shown in figure 12. The Hahn Echo relaxation delay was added before the carbon t_1 period when the operator N_zC_y was present. Although the ^{13}C-fraction on the β-position was reduced by selective labelling as was outlined in chapter 1.2.5, a shaped soft pulse was incorporated in the middle of the relaxation delay to refocus reminiscent $^{13}C_\alpha$ - $^{13}C_\beta$ coupling. The shaped soft pulse on C_α was a ReBurp.256 pulse with a bandwith of 26 ppm (1100 μs) at 6.24 dB (see fig. 7). To refocus coupling of $^{13}C_\alpha$ to the backbone nitrogens during the relaxation delay, two hard 180° pulses on nitrogen were put the center of the halved delay on both sides of the soft pulse. Coupling to the α-hydrogen was suppressed by a WALTZ-16 sequence. [28]

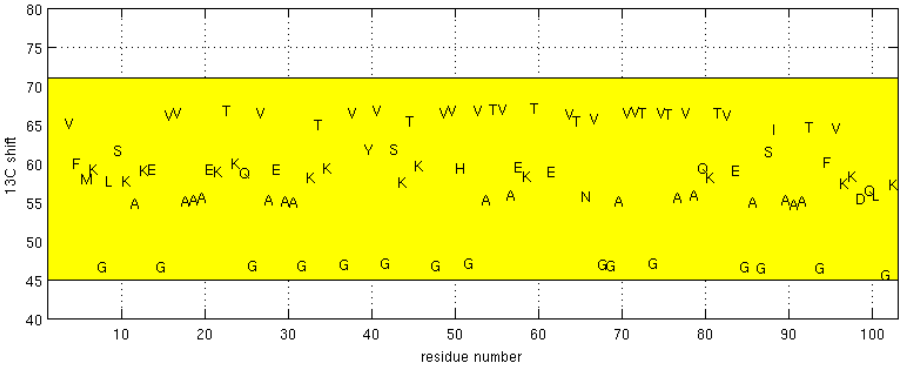

Figure 7 – Excitation bandwidth for 1100 μs ReBurp.256.

Spectra were taken from a ^{13}C and ^{15}N labelled sample on the 18.8 T Bruker Avance spectrometer equipped with triple resonance z-axis gradient cryoprobe at 323.5 K. The spectra were recorded with 64 scans per time point and 1024 x 512 time points in the direct / indirect dimension. The spectral width was set to 9615 Hz (12 ppm) for ^{1}H, 6713 Hz (26 ppm) for ^{13}C and 5830 Hz (65 ppm) for ^{15}N. The offset was set to 3763Hz (4.704 ppm) and 9327 Hz. The short and long relaxation delay of the Hahn Echo sequence were 0.2 and 30.58 ms and were recorded 2 and 3 times, respectively. The whole experiment was conducted twice.

Spectral processing in the time-domain was carried out using NMRPipe. [41] The free induction decays in both dimensions were multiplied by a cosine function, zero filled to double the number of points, fourier transformed and phase shifted to give in-phase spectra. In the indirect dimension, the data points were doubled using a forward-backward linear prediction with an order of 32.

Sparky was used to extract peak heights. [42] The peak heights of each experiment were averaged, fitted to a monoexonential decay in MATLAB and divided by the^{15}N R_1rate to

remove this contribution. [50] The relaxation rates of the C_i-N_i-H_i and C_i-$N_{(i+1)}$-$H_{(i+1)}$ data of both experiments were averaged (see fig. 8). In order to validate the averaging, paired t-tests with a Bonferroni correction for all permutations, to account for the alpha-factor-correction, was used. When using an alpha of 0.01 (1%), all calculated p-values are above the threshold and the means of the four data sets are statistically the same. The standard error was calculated and propagated according to NIST. [43]

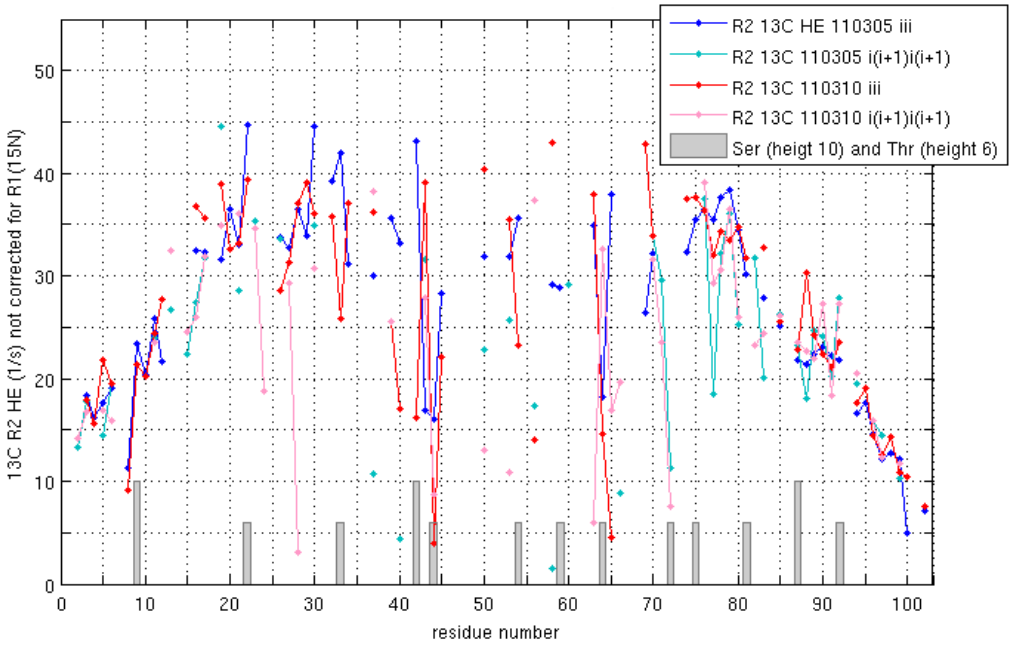

Figure 8 – ^{13}C R_2relaxation rates for the C_i-N_i-H_i and C_i-$N_{(i+1)}$-$H_{(i+1)}$ data of both experiments '110305' and '110310'. Serine and Threonine residues are labelled with gray bars.

Data points were excluded due to several reasons: 4% of possible peaks have not been assigned in the HNCA spectra and 20% of the peaks were too overlapped in the spectra so that no unambiguous rate could be calculated. About 8% of the peaks had a signal to noise (S/N) lower than 2. This cutoff was chosen so low, as the average S/N of residues 40 to 60 of the long relaxation delay was only 5.5. As glycines were quite at the edge of the soft pulse and have a different H_α-contribution due to the second attached hydrogen, they were also removed (10% of residues). In total there was no rate calculated for 26% of all residues (another quarter of residues had one or more individual data points excluded, but the rate and a corresponding standard error could be calculated).

Serine and Threonine have their C_β in the range which is also excited by the refocusing soft pulse during the long relaxation dealy. They are all marked in the figures, but were not

excluded as Takeuchi *et. al.*[51] found a clean labeling pattern for Serine (100% C_α labelling) and an intermediate labelling level for Threonine (60%). They have not measured the C_β percentage, but due to the metabolic pathways for Serine and Threonine it is reasonable to assume that roughly the fraction not labelled at the α-position, is labelled at the β-position. All Serines and Threonines are marked in the figures containing ^{13}C relaxation rates. Except for 2 Threonines (T44 and T72) they seem to fit quite well into the data surrounding them. Both of them have very low S/N, which might be the reason for the deviation.

To calculate the isotropic relaxation ratio $\frac{^{15}N(c_{DD}^2+c_{CSA}^2)}{^{13}C(c_{DD}^2)}$ (see Relaxation Mechanisms in 1.2.3), the magnetogyric ratios, vacuum permeability and Planck's constant were taken from Cavanagh *et. al.* [28], the N-H bond length from Yao *et. al.* [52], the C_α-H_α bond length from Case [53] and the chemical shift anisopy from Pandey *et. al.* [54].

3 Results

3.1 Protein Production

After induction, α-Synuclein accumulated steadily inside the cells, reaching a peak after 3-4 hours as seen in figure 9. α-Synuclein is not accumulated outside the cells, nor is there any significant cell lysis. The OD_{600} typically increased slightly, corresponding to a limited cell growth, as seen in the slight increase in overall band intensity of the pellet fraction.

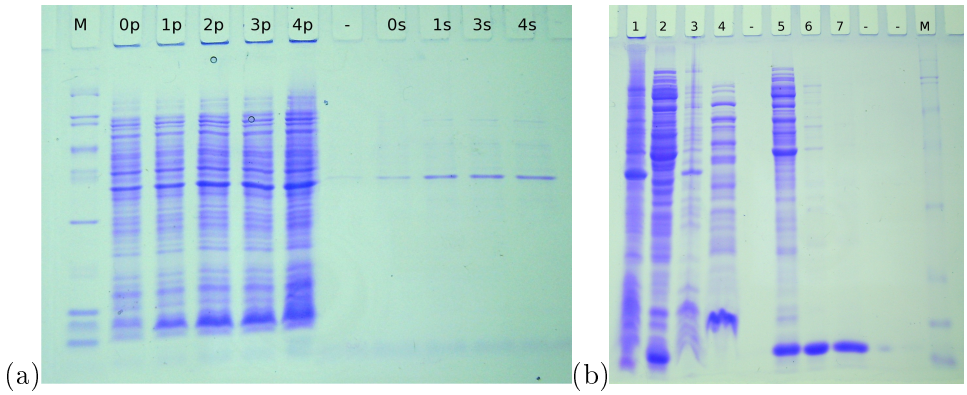

Figure 9 – Expression and purification overview. (a) Expression of α-Synuclein 102stop 0, 1, 2, 3 and 4h after inducion in the pellet fraction (p) and supernatant (s). Of the cell suspension, $1/50000^{th}$ of the total volume was spun down and separated into pellet and supernatant. On this gel, some α-synuclein swapped over into the marker lane during loading. (b) Overview of purification steps: Sonication pellet and supernatant (1, 2), Ultracentrifugation pellet and supernatant (3, 4), Ammonium sulfate pellet (5), pooled FPLC fractions (6) and pooled HPLC-fractions (7). In the case of liquid samples $1/5000^{th}$of the total volume was taken. The pellets are not quantitative. In the first/last of gel (a) and (b) lane, 7μl of Bio-Rad SDS-PAGE Broadrange Marker was run. The band sizes are 6.5, 14.4, 22, 31, 45, 66, 97, 116, and 200 kDa.

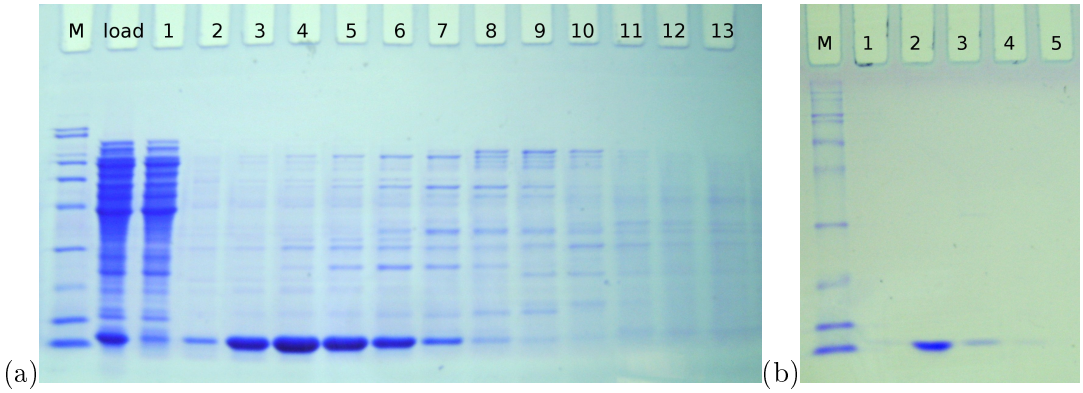

Figure 10 – Chromatographic purification steps. (a) FPLC-fractions (1-13) and loaded sample (load). (b) HPLC-fractions (1-5). On both gels 7μl of Bio-Rad SDS-PAGE Broadrange Marker was run in the first lane. The band sizes are 6.5, 14.4, 22, 31, 45, 66, 97, 116, and 200 kDa.

Sonication released the protein, which was separated by ultracentrifugation from the pelleted cell debris (see figure 9). The most efficient purification step is FPLC, which removes

most cellular proteins, without significantly reducing the quantity of α-Synuclein. After the last step. HPLC, there are no other bands than α-Synuclein visible on the gel. Typically, 5mg of lyophilized protein were obtained from the purification.

3.2 $^{13}C_{\alpha}$-Relaxation Experiment

The ^{13}C-HSQC was too overlapped to give enough resonance dispersion for relaxation experiments as shown in figure 11.

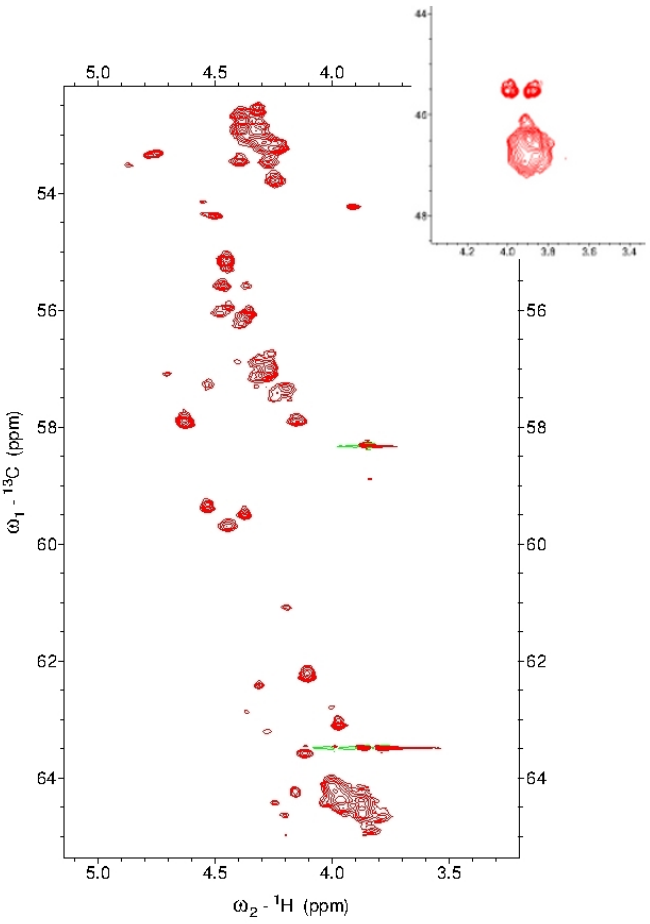

Figure 11 – Central region of a $^{13}C_{\alpha}$ PEP gHSQC spectrum. The glycines are in the insert in the upper right hand corner.

The reduced dimensionality HNCA-spectrum gave a reasonable signal dispersion which was optimised by altering the spectral contribution of nitrogen and carbon as shown in figure 12. In spectrum (a) the relative contribution from carbon is higher, so that it resembles more a $^{13}C_{\alpha}$–H_N spectrum. Spectrum (b) resembles slightly more a ^{15}N–$H_N$spectrum. Spectrum (a) gave a reasonable signal dispersion, so these td_1-intervals were chosen for the relaxation experiments.

The increments of this spectrum were 150 and 170 µs for ^{13}C and ^{15}N, corresponding to a spectral width of 6713 and 5830 Hz, respectively.

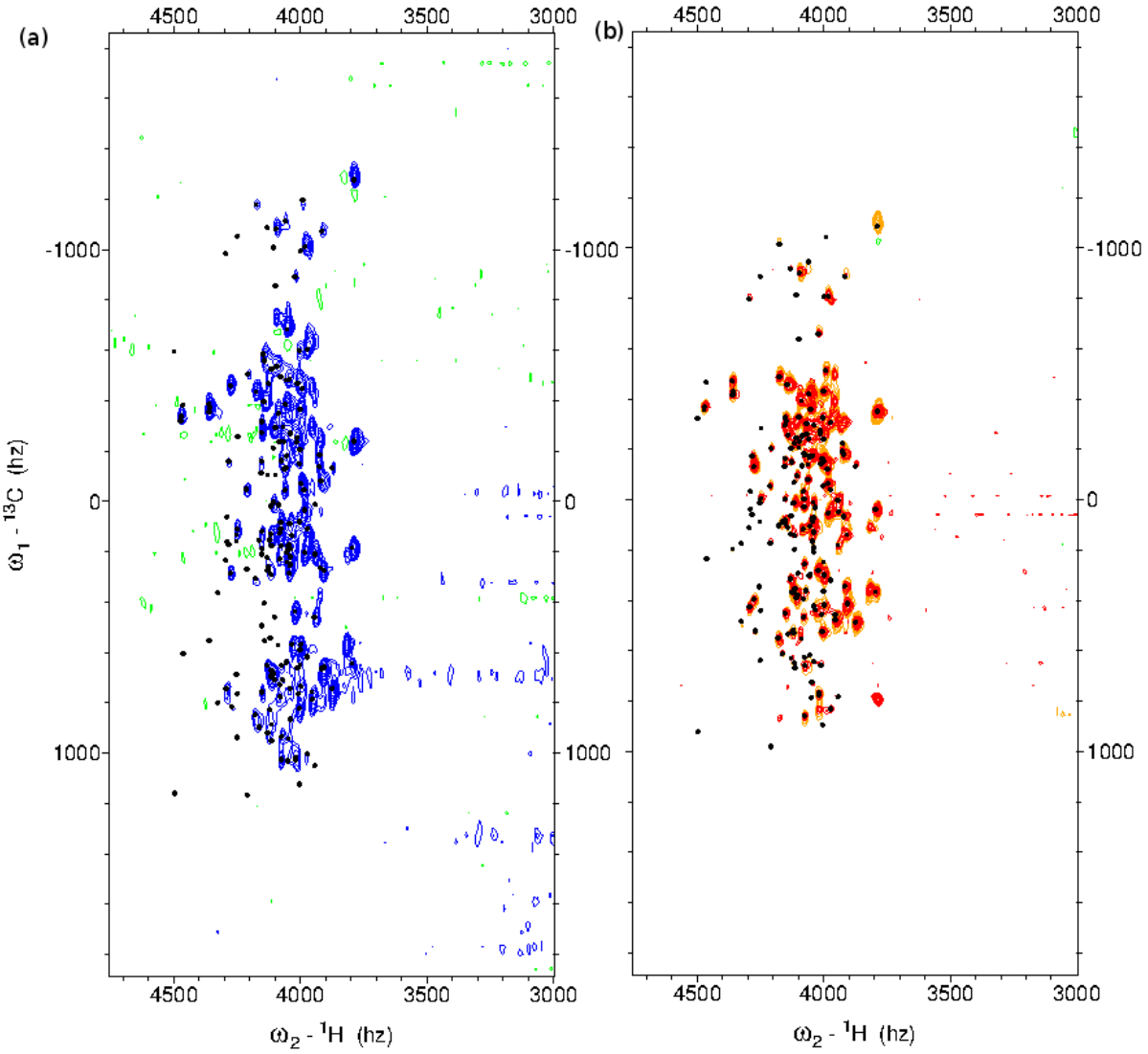

Figure 12 – Reduced dimensionality HNCA-spectra with varying contribution from nitrogen and carbon shifts. Measured spectra are compared against the expected, computed signals (black dots). (a) Spectrum with 6713 and 5830 Hz for ^{13}C and ^{15}N. Positive signals are blue, negative signals are green. (b) Spectrum with 3773 and 2178 Hz for ^{13}C and ^{15}N in red. Spectrum with 7547 and 4357 Hz for ^{13}C and ^{15}N in orange. The orange spectrum is folded, as the signal in the upper right hand corner is shifted into the lower right hand corner.

3.3 Helix Topology

3.3.1 Secondary $^{13}C_\alpha$ and ^{15}N Chemical Shifts

Secondary chemical shifts give information on the protein secondary structure and were used here to test for the helicity of the protein. The $^{13}C_\alpha$ secondary shifts are positive throughout

the peptide, corresponding to a helical structure throughout the protein (see fig. 13 (a)). Most ^{15}N secondary shifts are negative, and support therefore the hypothesized global helical structure as ^{15}N secondary shifts are strongly anticorrelated to the α-carbon shifts (see fig. 13 (b)). The correlation with secondray structure is less strong in the case of ^{15}N, explaining the few exeptions with positive chemical shifts dipersed throughout the protein.

The secondary shifts of free α-Synuclein do have a preponderance to slightly positive values, but this may only indicate nascent or transiently populated helical structure in a predominantly unstructured ensemble. [38] The measured secondary shifts show much more similarity to the $^{13}C_\alpha$ secondary shifts of α-Synuclein in SDS-micelles , except for the drop in secondary shifts found around residue 42. [8] Therefore the secondary values of α-Synuclein in HFIP support a continuous helical structure throughout the peptide.

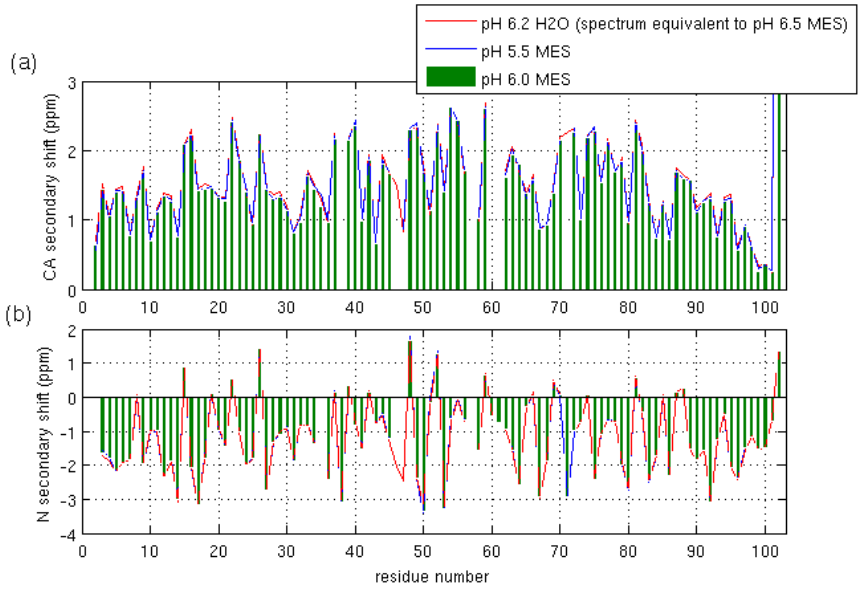

Figure 13 – Secondary chemical shifts at different pH-conditions. (a) $^{13}C_\alpha$ according to Mulder [27] and (b) ^{15}N according to Vendruscolo [26].

When investigating the protein at different pH-conditions, H50 and to a lesser extent the residues above and below were found to migrate to different ^{1}H- and ^{15}N-shifts. These residues exhibit a drop in ^{1}H-shifts with increasing pH. In the case of nitrogen the direction is consistent for a specific nucleus, but is not the same among different residues. When looking at the nitrogen secondary shifts of H50 and the residues directly above and below it was found that they do vary most compared to the other residues in the peptide, but even for H50 this only means a shift change of +0.27ppm in the tested pH-region. In order to investigate the pH-

effect on helicity, HNCA-spectra were recorded at three different pH-conditions. The carbon shifts do also vary most for H50, but the effect is even smaller (+0.11ppm). Therefore the chemical shift change does not arise from a change in secondary structure, but is presumably due to a change in charge as the pKa of Histidine is close to the tested pH-region.

3.3.2 Amide Nitrogen Relaxation

The transverse relaxation rates of the α-Synuclein ^{15}N backbone atoms are bell-shaped. They increase steeply symmetrically within about 15 residues up to 25 s^{-1}(500 MHz) and then show a steady moderate increase for the next 20 amino acids up to 30 s^{-1}(500 MHz), as shown in figure 14 (a). In the central region, the residues increase again, exhibiting the highest values. The drop in relaxation rates could arise from fast motions, e.g. due to helix fraying. The elevated relaxation rates in the center, could arise from conformational or chemical exchange, caused by helix bending or from temporary helix breaks. The bending causes a temporary disruption of hydrogen bonds and exchange of the hydrogen with water. In order to test this hypothesis, the R_2-Hahn Echo experiment was complemented by a R_2-CPMG experiment wich a pulsing frequency of 1000 Hz. The means of both data sets are statistically the same (paired t-test with alpha=0.05) and the motion/exchange - if present - must be either faster or slower than the ms-μs time regime covered by the CPMG-experiment.

The longitudinal ^{15}N relaxation rates of α-Synuclein symmetrically drop quickly within about 15 residues at both edges from 1.8 $s^{-1}$to 1.2 s^{-1}(500 MHz), as shown in figure 14 (b). In the remaining region, they continue to drop slowly to 1.1 s.

At 800 MHz the data resembles for $R_2$and $R_1$the same overall pattern, shifted only to lower relaxation rates. In the case of longitudinal relaxation this behavior is expected. In the case of the transverse relaxation this is surprising as from theory, the relaxation rates of macromolecules having $\tau_c > \frac{1}{\omega_c}$ are expected to increase with increasing field strength. A reason for this could be that the contribution from the longitudinal ^1H_Nrelaxation offsets the expected increase in transverse ^{15}N relaxation.

The diffusion tensor can give information about the molecular shape and was calculated from the ^{15}N R_1 and R_2-data imposed on a single straight helix using the program TENSOR2. [44] The results for an isotropic, axially symmetric and fully asymmetric diffusion tensor can be seen in table 1 and figure 15. However, upon confidence limit testing, all models

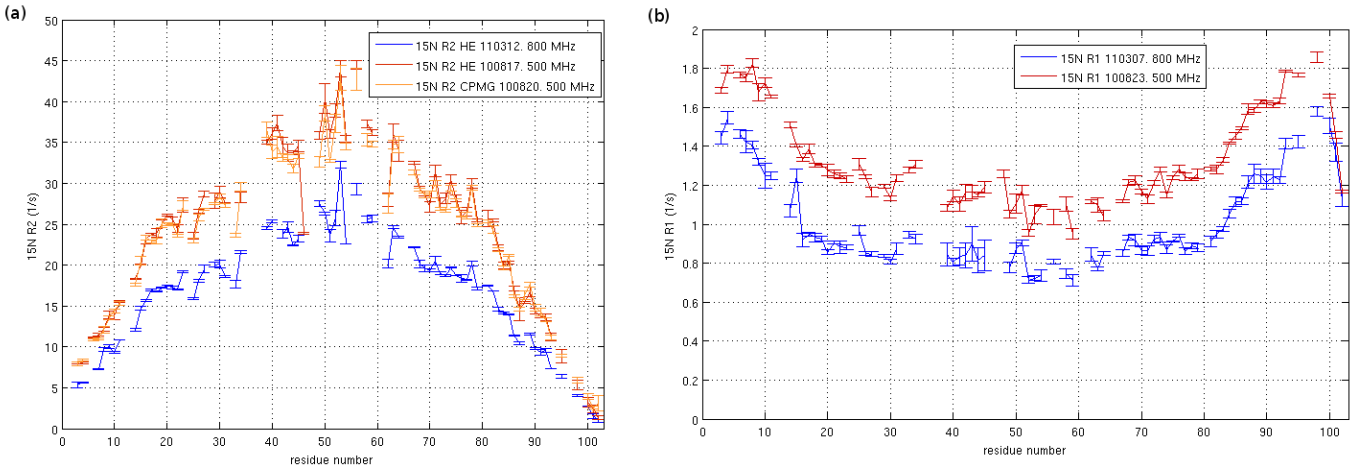

Figure 14 – $R_2$and $R_1$of backbone ^{15}N. (a) R_2Hahn Echo and CPMG at 500 and 800 MHz. The means of the Hahn Echo and the CPMG Experiment at 500MHz are statistically the same (α=0.05). (b) R_1 at 500 and 800 MHz. The relaxation rate decreases with increasing field strength.

are rejected as the experimental Chi^2-values are larger than the simulated optimal parameters. The pattern of the expected R_2/R_1 ratios for the individual residues do not resemble the measured relaxation rates, as seen in figure 15(c). Therefore, the $R_2(^{15}N)$ and $R_1(^{15}N)$ - data does not support the single straight helix-structure. As expected from the proposed structure, the space is sampled in a very limited range only (fig. 15(b)).

As the R_2/R_1ratios for residues 16-39 and 60-79 do not increase significantly, the data from this part of the peptide was subjected to the same diffusion tensor calculations (Data not shown here). Upon testing the confidence limits, all three models were also rejected.

Model	Parameters	Chi^2(Experimental)	Chi^2(0.05)
Isotropy	τ_c(s) 1.056e-8 ±1.213e-11	8.05e+4	1.03e+2
Axial Symmetry	$D_\parallel$ (1/s) 3.924e+6 ±2.163e+4 $D_\perp$ (1/s) 5.058e+7 ±1.968e+5	7.06e+4	9.99e+1
Full Asymmetry	D_{xx} (1/s) 7.180e+4±8.057e+3 D_{yy} (1/s) 8.458e+6 ±1.051e+5 D_{zz} (1/s) 4.454e+7 ±2.236e+5	6.92e+4	9.47e+1

Table 1 – Diffusion parameters and confidence limits for isotropic, axially symmetric and fully asymmetric diffusion calculated from ^{15}N R_1 and R_2-data imposed on a single straight helix.

Although the calculated correlation time τ_c does not withstand statistical verification, the approximate size may give some information. A globular molecule of 10.2 kDa in aqueous solution at 20°C, is expected to have a correlation time of about 6.1 ns. The experimentally determined correlation time of 10.6 ns is almost twice as big and would correspond to a protein

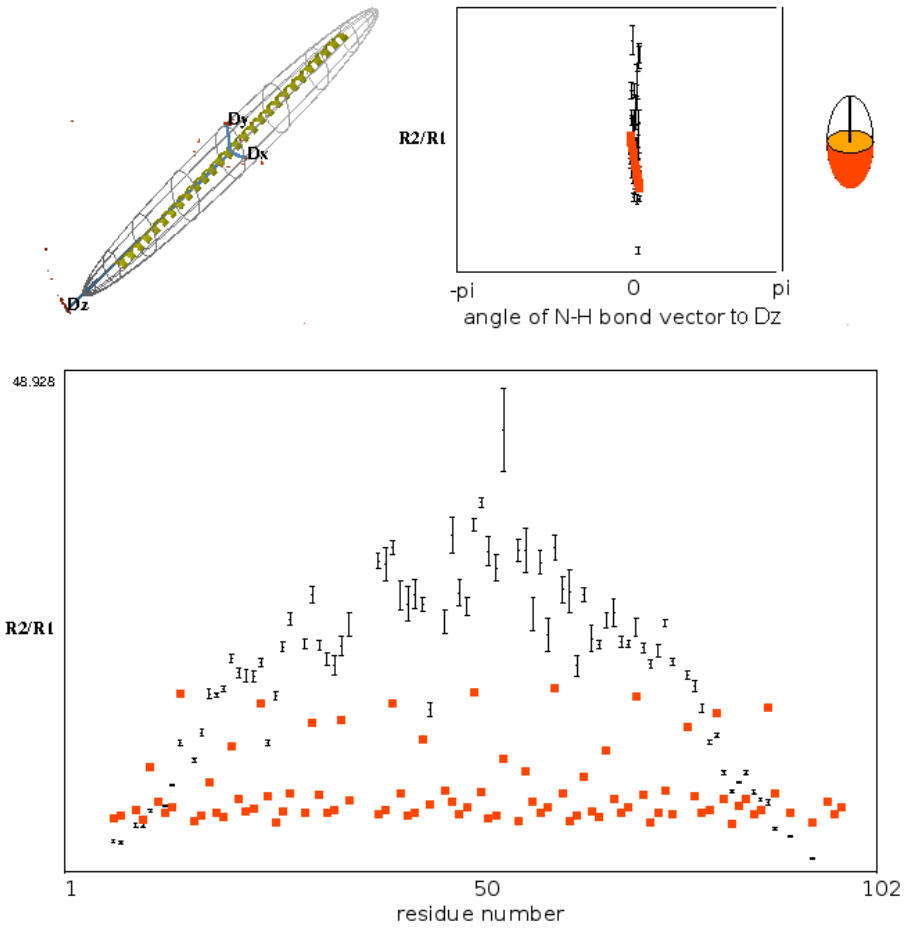

Figure 15 – Diffusion tensor calculated from ^{15}N R_1 and R_2-data imposed on a single straight helix. (a) Orientation of the three principal components of a fully asymmetric diffusion tensor. (b) Angular dispersion of N-H bond vectors compared to experimental (black) and theoretical (red) R_2/R_1 ratio. (c) Experimental (black) and calculated (red) R_2/R_1 ratio along the peptide backbone. All outliers which have higher calculated R_2/R_1 ratios compared the majority of residues lie on one face of the helix and their angles correspond particularly well with the orientation of the slightly tilted diffusion tensor. The slightly tilted diffusion tensor may arise from non-uniform exclusion of relaxation rates.

17.3 kDa in size. α-Synuclein in HFIP seems to be larger than expected for a globular protein (neglecting temperature and viscosity-effects). When accounting for both environmental effects, the hydrodynamic radius of α-Synuclein is 27 Å, that of a globular protein with the same molecular weight would be 23 Å. Therefore α-Synuclein is less compact than a globular protein, but presumably more compact than a single straight helix which would be a cylinder of 150x12 Å.

3.3.3 α-Carbon R_2 Relaxation

The pattern of the $^{13}C_\alpha$ R_2 relaxation rates follows roughly the pattern of the ^{15}N residues, as shown in figure 16. The rates at the edges are low, indicating possibly fast motion contributions. They increase within about 15 residues to a plateau at 30-35 s^{-1}, relaxing on average about 15 s^{-1}faster than nitrogen. In the centre, there is a drop in $^{13}C_\alpha$relaxation rates, the opposite trend compared to the elevated relaxation rates of the nitrogen-data. This could indicate that the helix is less stable in the central region so that the α-carbons at this temporary bend/break experience a difference in motion.

However, the drop in relaxation rates in the centre may also arise from the low S/N in the central region, which would decrease the rates artificially. Also the low rate of L8 could be attributed to this S/N- effect, as Leucines have the lowest C_α and highest C_β labelling fraction among the amino acids. [51] The second Leucine in the sequence (L38) did not give enough signal to measure a rate and the third Leucine (L100) is in the C-terminal region of the protein, which has the highest S/N of the peptide and does not have a markedly different rate compared to the surrounding residues. In order to rule out the S/N-effect, the ^{13}C experiments would need to be repeated and the number of scans or td_1-points increased to give an overall better S/N ratio.

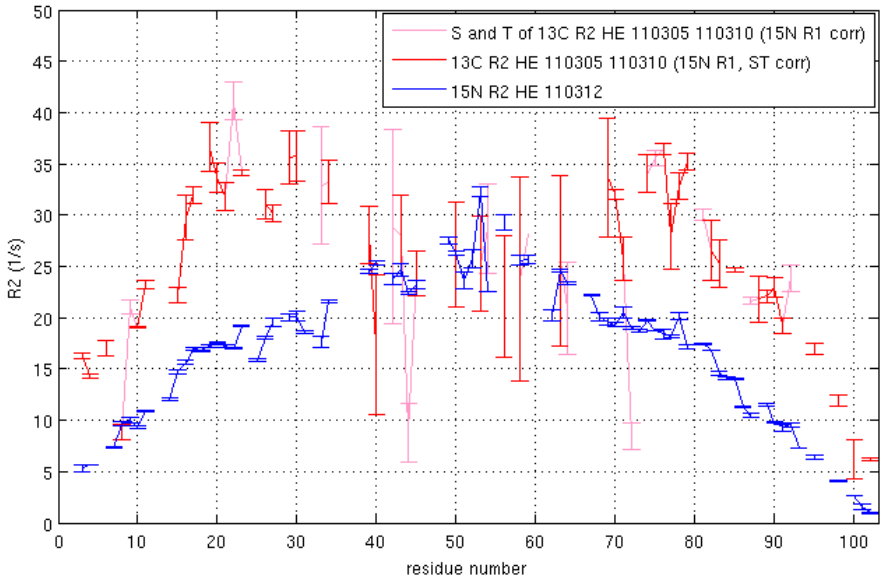

Figure 16 – R_2 of ^{13}C and^{15}N at 800 MHz. The pattern of the relaxation data for the flanking residues is the same. Only the central region is markedly different. Serines and Threonines are marked in pink.

When making a scatter plot comparing ^{13}C rates and ^{15}N rates, three groups were found.

Residues 1-15 and 80-102 lie quite well on a straight line with a slope of 0.59 $R_2(^{15}N/^{13}C)$. Therefore, the carbon relaxation increases 1.5fold quicker compared to the 15N relaxation, pointing at a stable helical element in this region. The other two groups form heaps. Residues 16-39 and 60-79 form a bundle elongating the straight line of the terminal residues, indicating a continuation of the helix where the elongation effects may not be that pronounced any more. Residues 40-59 do not form a continuation of this trend. They are situated above them due to their elevated 15N rates, but shifted towards the left due to the lower Ca rates.

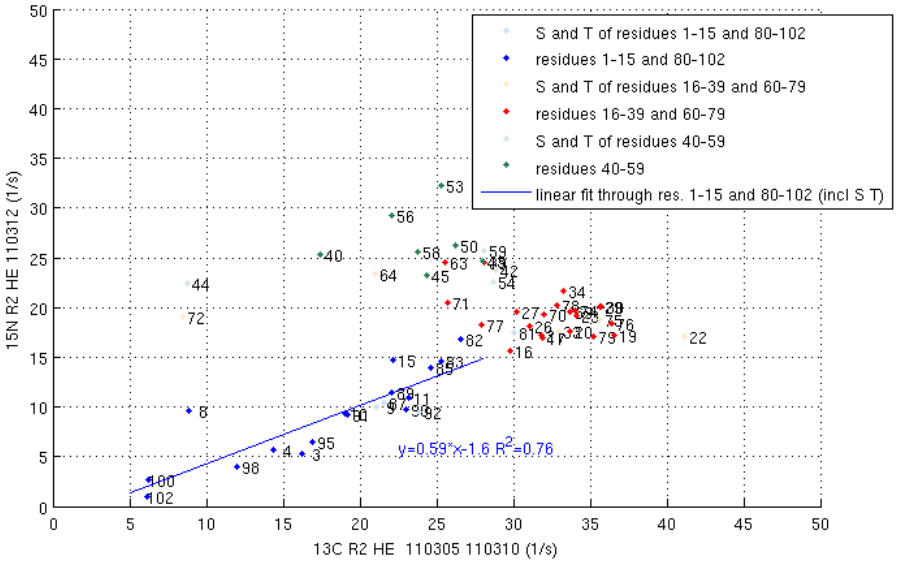

Figure 17 – Scatter plot of R_2 of ^{13}C and^{15}N at 800 MHz, showing three distinct regions. Residues 1-15 and 80-102 form a straight line. Residues 16-39 and 60-79 and residues 40-59 build two groups. Serines and Threonines are marked in lighter colors.

To test the hypothesis whether the ^{15}N-H and $^{13}C_\alpha$-H bond vectors experience the predicted difference in motion, the ratio of ^{15}N to ^{13}C R_2relaxation rates was calculated for all residues. When comparing this ratio to the R_2 relaxation ratio expected for isotropic tumbling (0.789), most residues lie below this value, i.e. $^{13}C_\alpha$ in α-synuclein relaxes faster and tumbles slower than expected in an isotropic molecule. This observed anisotropy is in fact opposite to the ratio that would be expected for a single straight helix.

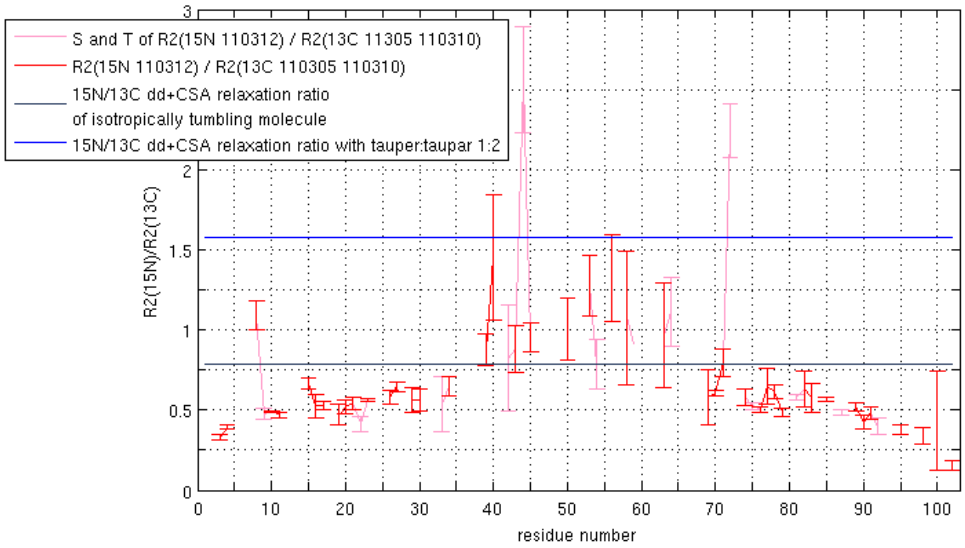

Figure 18 – R_2 ratio of ^{15}N to^{13} C at 800 MHz compared to theoretical ratio for isotropically tumbling molecule and for a molecule with $\tau_\perp$:$\tau_\parallel$ 1:2. Serines and Threonines are marked in pink.

4 Discussion

The secondary shifts of α-Synuclein strongly argue for a continuous helix and against a break, as was found for α-Synuclein in SDS-micelles. However, the data from the $R_2(^{15}N/^{13}C)$ ratios as well as the diffusion tensor calculated from the $R_2(^{15}N)/R_1(^{15}N)$ data do not support the hypothesis of a single straight helix. Instead, the shape of the molecule does not resemble the proposed prolate, but rather an oblate or something alike. There are three possible explanations for this finding:

1) α-Synuclein is known to adopt oligomeric assemblies in solution. [55], [56] This might be also the case in 30% HFIP, distorting the overall shape of the aggregate. The extrapolated molecular weight of the determined correlation time (10.6 ns, 17.3 kDa) is smaller than expected for an oligomeric species, making this option less likely for the conditions used in the study. However, the uncertainty in the correlation time is very high, attenuating the strength of the argument.

2) HFIP has been shown to coat molecules and form micro-clusters in aqueous solution. [24] Thereby, the proposed elongated shape of the molecule would be distorted and the tumbling less anisotropic. This difference in shape leads to a more isotropic rotation behaviour than a single straight helix.

3) The helix may be indeed bent or broken. A break is not supported by the secondary

shift data, but the breaking may well be transient. A transient break or a bent helix is actually supported by the relaxation data of both tested nuclei. The increased $R_2(^{15}N)$ in the center may be attributed to conformational or chemical exchange. When trying to get information on the timescale of this proposed motion, it was found that it is not on a timescale covered by the CPMG-experiment (ms-μs). The $R_2(^{13}C)$ decreases in the center of the peptide, pointing at a different motional regime experienced by this region. However, the S/N of these residues is very low and it cannot be completely ruled out that this is effect is an artefact.

In the literature there are two published helical structures of α-Synuclein (1XQ8 [11] and 2KKW [12]) studied by NMR and EPR. Both are in association with micelles (SDS and SLAS) and the protein engulfs the micelles by two antiparallel helices. In the case of 1XQ8, the curved helices span from Val3-Val37 and Lys45-Thr92, connected by a well ordered linker. The structure of 2KKW is alike, in that the helices span residues Asp2-Lys32 and Ser42-Thr92. The C-terminal tails are in both cases unstructured. Extracting the coordinates for residues 1-102 of the two structures and fitting the measured relaxation data of α-Synuclein in 30% HFIP to it, the diffusion parameters displayed in table 2 and figure 19 were calculated.

Protein / Model	Parameters		Chi^2(Experimental)	Chi^2(0.05)
1XQ8				
Isotropy	τ_c(s)	8.789e-9 ±1.167e-11	8.06e+4	1.05e+2
Axial Symmetry	$D_\parallel$ (1/s)	2.618e+5 ±1.377e+5	5.70e+4	1.01e+2
	$D_\perp$ (1/s)	3.868e+7 ±2.319e+5		
Full Asymmetry	Dx (1/s)	3.843e+4±1.481e+4	5.45e+4	1.01e+2
	Dy (1/s)	2.927e+7 ±2.080e+5		
	Dz (1/s)	4.660e+7 ±3.117e+5		
2KKW				
Isotropy	τ_c(s)	8.789e-9 ±9.224e-12	8.06e+4	1.02e+2
Axial Symmetry	$D_\parallel$ (1/s)	2.581e+6 ±8.635e+3	5.70e+4	1.09e+2
	$D_\perp$ (1/s)	2.090e+8 ±1.730e+6		
Full Asymmetry	Dx (1/s)	5.674e+4±2.115e+4	5.64e+4	1.05e+2
	Dy (1/s)	3.203e+7 ±3.027e+5		
	Dz (1/s)	6.341e+7 ±5.420e+5		

Table 2 – Diffusion parameters and confidence limits for isotropic, axially symmetric and fully asymmetric diffusion. They were calculated from ^{15}N R_1 and R_2-data imposed on 1XQ8 and 2KKW.

As was the case with the single straight helix, all of the models are rejected, as the experimental Chi^2-values are larger than the simulated optimal parameters. Therefore, the actual structure of α-Synuclein in 30% HFIP differs from the micelle-bound structures of α-

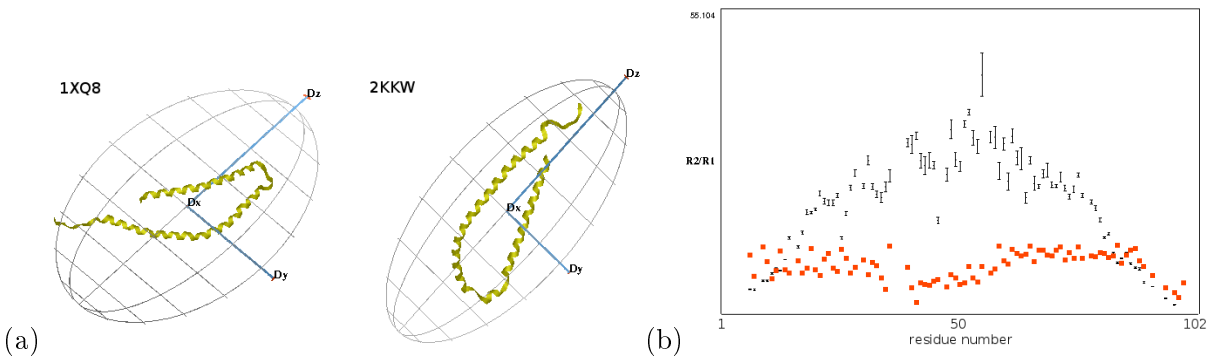

Figure 19 – Fully asymmetric diffusion tensors of the PDB-structures 1XQ8 and 2KKW and the ^{15}N R_1 and R_2-data. (a) Graphical display of the diffusion tensor. Only residues 1-102 were taken from each structure for the fitting and are depicted here. (b) Comparison of R_2/R_1 data (black) for the diffusion tensor calculations to the calculated ratio of 2KKW (red) along the peptide backbone. There is a good agreement for residues Ala85-Lys102.

Synuclein. The observed break in α-Synuclein in micelles has, in fact, already been attributed several times to being an effect of the size of micelles and is according to the data presented here not present in α-Synuclein in 30% HFIP. [6]

When analysing the data in detail, it was noticed, that the R_2/R_1 data of Ala85-Lys102 of 2KKW corresponds well to the expected data of the structure (see fig. 19). This could indicate that the curvature of this end of the helix in 2KKW matches the curvature of this region of α-Synuclein in 30% HFIP.

Recently, Braun et. al. published an article on the induction of membrane curvature by α-Synuclein (residues 1-100). [1] They also studied a truncated version of α-Synuclein by a combination of X-ray scattering, fluorescence correlation spectroscopy, coarse-grained MD simulations and potential of mean force calculations. These multiple approaches led to the conclusion that α-Synuclein stabilizes a positive mean curvature, such that the maximum principle curvature matches that of synaptic vesicles (see fig. 20).

The data presented in this thesis, does fit well to a bent helix and it may well be the case that α-Synuclein in 30% HFIP adopts a similar structure as was found for α-Synuclein in a membrane by Braun *et. al.*. [1] As there is no PDB-structure available of the bent α-Synuclein, it is not possible to fit and evaluate the diffusion tensor against this structure. However, the continuous helicity of the secondary shifts and the rise of the central $R_2(^{15}N)$ rates may be explained by this structure. Also the drop in the central $R_2(^{13}C)$ rates may be attributed to this structure.

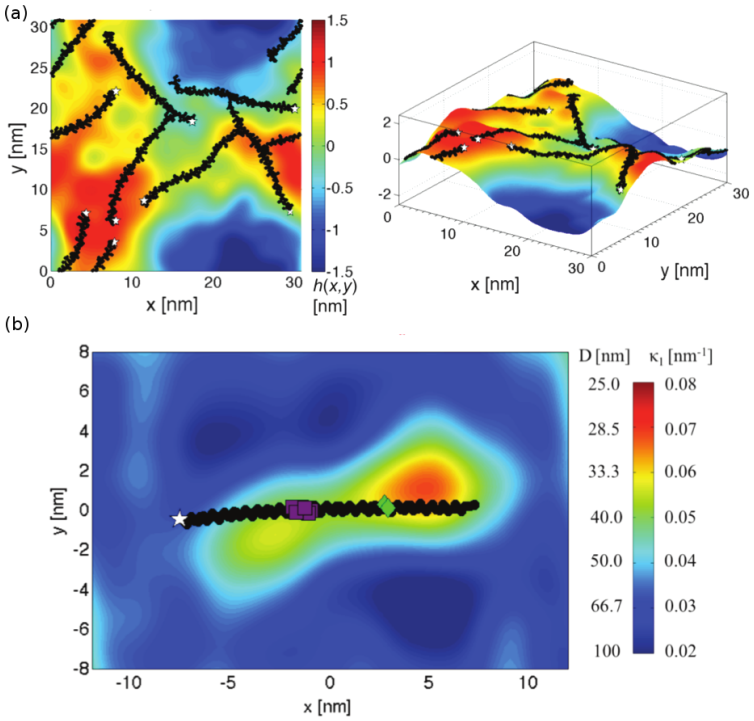

Figure 20 – α-Synuclein stabilizes positive mean curvature. (a) Representative height surface for the outer leaflet. The space is depicted as 2D-surface (x and y in nm), the height (h in nm) is represented as color gradient and the N-terminus of each protein is marked by a star. (b) Local curvature ($\varkappa_1$ in 1/nm) and corresponding vesicle diameter (D in nm). Purple squares indicate the linker region and the green tilted square indicates Gly67-Gly68. Taken from [1]

5 Conclusions

α-Synuclein in 30% hexafluoroisopropanol is according to the secondary shifts presented here a continuous helix. It is according to the data from the $R_2(^{15}N/^{13}C)$ ratios as well as the diffusion tensor calculated from the $R_2(^{15}N)/R_1(^{15}N)$ not straight. There are three possible explanations for a distortion in the overall shape.α-Synuclein may be present as oligomeric assembly. The calculated correlation time does argue against this possibility, although the strength of the argument is attenuated by the high uncertainty of the correlation time. HFIP in aqueous solution coats molecules and forms microclusters. Thirdly, the helix may be transiently broken or bent. The motional regime of this possible breaking was found to be either faster or slower than the common timescale of this motion, covered by the CPMG-experiment (ms-µs). The data presented in this thesis, does fit well to a bent helix and it may well be the case that α-Synuclein in 30% HFIP adopts a similar structure as was found recently for α-Synuclein in a membrane by Braun *et. al.* .[1]

6 References

References

[1] Anthony R. Braun, Eva Sevcsik, Pamela Chin, Elizabeth Rhoades, Stephanie Tristram-Nagle, and Jonathan N. Sachs. a-synuclein induces both positive mean curvature and negative gaussian curvature in membranes. *Journal of the American Chemical Society*, 134(5):2613–2620, February 2012.

[2] Hilal A. Lashuel, Cassia R. Overk, Abid Oueslati, and Eliezer Masliah. The many faces of α-synuclein: from structure and toxicity to therapeutic target. *Nature Reviews Neuroscience*, 14(1):38–48, December 2012.

[3] L Stefanis. α-synuclein in parkinson's disease. *Cold Spring Harb Perspect Med*, 4:a009399:1–23, 2012.

[4] S. Chandra. Double-knockout mice for - and -synucleins: Effect on synaptic functions. *Proceedings of the National Academy of Sciences*, 101(41):14966–14971, October 2004.

[5] J. Burre, M. Sharma, T. Tsetsenis, V. Buchman, M. R. Etherton, and T. C. Sudhof. a-synuclein promotes SNARE-Complex assembly in vivo and in vitro. *Science*, 329(5999):1663–1667, August 2010.

[6] Igor Dikiy and David Eliezer. Folding and misfolding of alpha-synuclein on membranes. *Biochimica et Biophysica Acta (BBA) - Biomembranes*, 1818(4):1013–1018, April 2012.

[7] Alexander S. Maltsev, Jinfa Ying, and Ad Bax. Impact of n-terminal acetylation of α-synuclein on its random coil and lipid binding properties. *Biochemistry*, 51(25):5004–5013, June 2012.

[8] Robert Bussell Jr and David Eliezer. A structural and functional role for 11-mer repeats in ?-synuclein and other exchangeable lipid binding proteins. *Journal of Molecular Biology*, 329(4):763–778, June 2003.

[9] Pavan K. Auluck, Gabriela Caraveo, and Susan Lindquist. α-synuclein: Membrane interactions and toxicity in parkinson's disease. *Annual Review of Cell and Developmental Biology*, 26(1):211–233, November 2010.

[10] S. Chandra. A broken alpha -helix in folded alpha -synuclein. *Journal of Biological Chemistry*, 278(17):15313–15318, February 2003.

[11] T. S. Ulmer. Structure and dynamics of micelle-bound human -synuclein. *Journal of Biological Chemistry*, 280(10):9595–9603, December 2004.

[12] Jampani Nageswara Rao, Christine C. Jao, Balachandra G. Hegde, Ralf Langen, and Tobias S. Ulmer. A combinatorial NMR and EPR approach for evaluating the structural ensemble of partially folded proteins. *Journal of the American Chemical Society*, 132(25):8657–8668, June 2010.

[13] Peter Borbat, Trudy F. Ramlall, Jack H. Freed, and David Eliezer. Inter-helix distances in lysophospholipid micelle-bound α-synuclein from pulsed ESR measurements. *Journal of the American Chemical Society*, 128(31):10004–10005, August 2006.

[14] Elka R. Georgieva, Trudy F. Ramlall, Peter P. Borbat, Jack H. Freed, and David Eliezer. Membrane-bound α-synuclein forms an extended helix: Long-distance pulsed ESR measurements using vesicles, bicelles, and rodlike micelles. *Journal of the American Chemical Society*, 130(39):12856–12857, October 2008.

[15] C. C. Jao, B. G. Hegde, J. Chen, I. S. Haworth, and R. Langen. Structure of membrane-bound -synuclein from site-directed spin labeling and computational refinement. *Proceedings of the National Academy of Sciences*, 105(50):19666–19671, December 2008.

[16] A. C. M. Ferreon, Y. Gambin, E. A. Lemke, and A. A. Deniz. Interplay of -synuclein binding and conformational switching probed by single-molecule fluorescence. *Proceedings of the National Academy of Sciences*, 106(14):5645–5650, March 2009.

[17] Daniel Russel, Keren Lasker, Jeremy Phillips, Dina Schneidman-Duhovny, Javier A. Velázquez-Muriel, and Andrej Sali. The structural dynamics of macromolecular processes. *Current Opinion in Cell Biology*, 21(1):97–108, February 2009.

[18] Christina R. Bodner, Christopher M. Dobson, and Ad Bax. Multiple tight phospholipid-binding modes of α-synuclein revealed by solution NMR spectroscopy. *Journal of Molecular Biology*, 390(4):775–790, July 2009.

[19] Rahul Rajan and P Balaram. A model for the interaction of trifluoroethanol with peptides and proteins. *INTERNATIONAL JOURNAL OF PEPTIDE & PROTEIN RESEARCH*, 48:328–336, 1996.

[20] I. Fadhil. Exploring deltorphin II binding to the third extracellular loop of the -opioid receptor. *Journal of Biological Chemistry*, 279(20):21069–21077, March 2004.

[21] Hongyan Li, Fei Li, Hongzhe Sun, and Zhong Ming Qian. Membrane-inserted conformation of transmembrane domain 4 of divalent-metal transporter. *Biochemical Journal*, 372(3):757, June 2003.

[22] Matthias Buck. Trifluoroethanol and colleagues: cosolvents come of age. recent studies with peptides and proteins. *Quarterly Reviews of Biophysics*, 31(2):297–355, 1998.

[23] Dong-Pyo Hong, Masaru Hoshino, Ryoichi Kuboi, and Yuji Goto. Clustering of fluorine-substituted alcohols as a factor responsible for their marked effects on proteins and peptides. *Journal of the American Chemical Society*, 121(37):8427–8433, September 1999.

[24] Daniel Roccatano. Computer simulations study of biomolecules in non-aqueous or Co-solvent/Water mixture solutions. *Current Protein and Peptide Science*, 9(4):407–426, 2008.

[25] D. S. Wishart, B. D. Sykes, and F. M. Richards. The chemical shift index: a fast and simple method for the assignment of protein secondary structure through NMR spectroscopy. *Biochemistry*, 31(6):1647–1651, February 1992.

[26] Alfonso De Simone, Andrea Cavalli, Shang-Te Danny Hsu, Wim Vranken, and Michele Vendruscolo. Accurate random coil chemical shifts from an analysis of loop regions in native states of proteins. *Journal of the American Chemical Society*, 131(45):16332–16333, November 2009.

[27] Kamil Tamiola, Burc?in Acar, and Frans A. A. Mulder. Sequence-specific random coil chemical shifts of intrinsically disordered proteins. *Journal of the American Chemical Society*, 132(51):18000–18003, December 2010.

[28] John Cavanagh. *Protein NMR spectroscopy: principles and practice*. Academic Press, Amsterdam ; Boston, 2nd ed edition, 2007.

[29] JW Peng and G Wagner. Investigation of protein motions via relaxation measurements. *Methods in Enzymology*, 239:563–596, 1994.

[30] Paolo Rossi, G. V. T. Swapna, Yuanpeng J. Huang, James M. Aramini, Clemens Anklin, Kenith Conover, Keith Hamilton, Rong Xiao, Thomas B. Acton, Asli Ertekin, John K. Everett, and Gaetano T. Montelione. A microscale protein NMR sample screening pipeline. *Journal of Biomolecular NMR*, 46(1):11–22, November 2009.

[31] D. E. Woessner. Nuclear spin relaxation in ellipsoids undergoing rotational brownian motion. *The Journal of Chemical Physics*, 37(3):647, 1962.

[32] J Kowalewski and L Mäler. *Nuclear Spin Relaxation in Liquids: Theory, Experiments and Applications*. Taylor & Francis Group, Florida, 1st ed. edition, 2006.

[33] Nico Tjandra, Scott E. Feller, Richard W. Pastor, and Ad Bax. Rotational diffusion anisotropy of human ubiquitin from 15N NMR relaxation. *Journal of the American Chemical Society*, 117(50):12562–12566, December 1995.

[34] LK Lee, M Rance, WJ Chazin, and AG III Palmer. Rotational diffusion anisotropy of proteins from simultaneous analysis of 15N and 13Ca nuclear spin relaxation. *Journal of Biomolecular NMR*, 9:287–298, 1997.

[35] Jeremy M. Berg, John L. Tymoczko, Lubert Stryer, and Lubert Stryer. *Biochemistry*. W.H. Freeman, New York, 5th ed edition, 2002.

[36] David M. LeMaster and Diana M. Kushlan. Dynamical mapping of e. coli thioredoxin via 13C NMR relaxation analysis. *Journal of the American Chemical Society*, 118:9255–9264, January 1996.

[37] Koh Takeuchi, Zhen-Yu J. Sun, and Gerhard Wagner. Alternate 13C-12C labeling for complete mainchain resonance assignments using c? direct-detection with applicability toward fast relaxing protein systems. *Journal of the American Chemical Society*, 130:17210–17211, December 2008.

[38] David Eliezer, Esin Kutluay, Robert Bussell Jr, and Gillian Browne. Conformational properties of ?-synuclein in its free and lipid-associated states1. *Journal of Molecular Biology*, 307:1061–1073, April 2001.

[39] Kelly A. Conway, James D. Harper, and Peter T. Lansbury. Accelerated in vitro fibril formation by a mutant a-synuclein linked to early-onset parkinson disease. *Nature Medicine*, 4:1318–1320, November 1998.

[40] C Ammann, P Meier, and AE Merbach. A simple multinuclear NMR thermometer. *Journal of Magnetic Resonance*, 46:319–321, 1982.

[41] F Delaglio, S Grzesiek, G Vuister, G Zhou, J Pfeifer, and A Bax. NMRPipe: a multidimensional spectral processing system based on UNIX pipes. *Journal of Biomolecular NMR*, 6:277–293, 1995.

[42] TD Goddard and DG Kneller. SPARKY 3. *University of California, San Fancisco.*

[43] H. H. Ku. Notes on the use of propagation of error formulas. *Journal of Research of the National Bureau of Standards*, 70C(4):262, October 1966.

[44] P Dosset, D Marion, and M Blackledge. TENSOR2, version jan 2001. institut de biologie structurale J.P. EBEL CEA-CNRS, grenoble, france.

[45] PyMOL molecular graphics system, version 1.3, schr{\"o}dinger, LCC., 2010.

[46] RCSB protein data bank - RCSB PDB. http://www.rcsb.org/pdb/static.do?p=general_information/news_

[47] DuPont. Hexafluoroisopropanol DuPont polymer specialties. http://www2.dupont.com/Polymer_Specialties/en_US/products/hfa_derivatives/hfip.html, February 2013.

[48] Maryadele J. O'Neil. *The Merck index.* Merck, Whitehouse Station, N.J, 14th ed edition, 2006.

[49] T. Szyperski, G. Wider, J. H. Bushweller, and K. Wuethrich. Reduced dimensionality in triple-resonance NMR experiments. *Journal of the American Chemical Society*, 115(20):9307–9308, October 1993.

[50] The Mathworks Inc. MATLAB version 7.11.0.584 (R2010b), 2010.

[51] Koh Takeuchi, Dominique P. Frueh, Zhen-Yu J. Sun, Sebastian Hiller, and Gerhard Wagner. CACA-TOCSY with alternate 13C–12C labeling: a 13C? direct detection experi-

ment for mainchain resonance assignment, dihedral angle information, and amino acid type identification. *Journal of Biomolecular NMR*, 47(1):55–63, April 2010.

[52] Lishan Yao, Beat Vo?geli, Jinfa Ying, and Ad Bax. NMR determination of amide N-H equilibrium bond length from concerted dipolar coupling measurements. *Journal of the American Chemical Society*, 130(49):16518–16520, December 2008.

[53] DA Case. Calculations of NMR dipolar coupling strengths in model peptides. *Journal of Biomolecular NMR*, 15:95–102, 1999.

[54] Manoj Kumar Pandey, Subramanian Vivekanandan, Shivani Ahuja, Kumar Pichumani, Sang-Choul Im, Lucy Waskell, and Ayyalusamy Ramamoorthy. Determination of 15 n chemical shift anisotropy from a membrane-bound protein by NMR spectroscopy. *The Journal of Physical Chemistry B*, 116(24):7181–7189, June 2012.

[55] W. Wang, I. Perovic, J. Chittuluru, A. Kaganovich, L. T. T. Nguyen, J. Liao, J. R. Auclair, D. Johnson, A. Landeru, A. K. Simorellis, S. Ju, M. R. Cookson, F. J. Asturias, J. N. Agar, B. N. Webb, C. Kang, D. Ringe, G. A. Petsko, T. C. Pochapsky, and Q. Q. Hoang. A soluble a-synuclein construct forms a dynamic tetramer. *Proceedings of the National Academy of Sciences*, 108(43):17797–17802, October 2011.

[56] Tim Bartels, Joanna G. Choi, and Dennis J. Selkoe. α-synuclein occurs physiologically as a helically folded tetramer that resists aggregation. *Nature*, 477(7362):107–110, August 2011.

7 Abbreviations

ESR Electron spin resonance

FRET Foerster resonance energy transfer

MD molecular dynamics

NMR nuclear magnetic resonance

OD optical density

RT room temperature

S/N signal to noise

Eidesstattliche Erklärung

Ich erkläre hiermit an Eides Statt, daß ich die vorliegende Arbeit selbständig und ohne Benutzung anderer als der angegebenen Hilfsmittel angefertigt habe. Die aus fremden Quellen direkt oder indirekt ubernommenen Gedanken sind als solche kenntlich gemacht

Die Arbeit wurde bisher in gleicher oder ähnlicher Form keiner anderen a Prüfungsbehörde vorgelegt und auch noch nicht veröffentlicht.

Wien, am 25.2.2013

(Cornelia Haas)

Cornelia Haas

Curriculum Vitae

Email cornelia.haas@gmx.at

Employment

Economic Research on Environmental Technology – Scientific Staff

University of Natural Resources and Life Sciences (BOKU), Department for Sustainable Economic Development, Vienna. Economic feasibility study for the production of chemicals and value-added foodstuff from wheat bran. The results of this study are now being implemented as a Christian-Doppler-Laboratory on a Bran-Biorefinery, a cooperation between the BOKU, the GoodMills Group and Buehler. 06/2011-12/2011

Biophysics – Scientific Staff

Columbia University, Department of Biophysics, und Cornell University, Department of Biochemistry, New York, USA. Development of a method and computer-based data analysis of complex molecular movements via Protein-NMR-Spectroscopy. Parts of this project are used as my Master thesis. 09/2009-03/2011

Molecular Biology – Part-time Scientific Staff

Medical University of Vienna, Austria, Division for special Gynecology. Conduction of a cancer research projects (cell culture, RNA methods, real time-PCR, immuno-histochemistry). 02/2006 - 03/2007

Philosophy of Science - Student Tutor

University of Vienna, Austria, Department of Social Studies of Science. Tutoring undergraduate and graduate students in seminars. 10/2005 - 01/2006

Skills

Languages

- German (native speaker)
- English (fluent oral, verbal and written, TOEFL iBT-score 116/120)

IT Skills

Excellent command of Windows and MS Office, Working knowledge of Linux (Ubuntu, shell scripting, Open Office), Matlab, GAMS, LSM II, Microfit

Education

Biological Chemistry, MSc

University of Vienna, Austria, coursework completed with highest honors
Master thesis: 'Rotational Anisotropy of α-helical α-Synuclein studied by ^{15}N and ^{13}C NMR-relaxation', Columbia University und Cornell University, USA, Grant for short-term scientific placements from the University of Vienna

Molecular Biology, BSc

University of Vienna, Austria, graduation 08/2008, Grant from the Julius-Raab Stiftung
Bachelors Project: 'Expression and Purification of a Selectively Labeled KIX Domain from CREB Binding Protein for NMR Structural Studies', University of Vienna, Dept. for Biomolecular Structural Chemistry

Chemical Sciences, BSc

Dublin Institute of Technology, Ireland, graduation with highest honors 02/2005
Bachelors Project: 'Assessment of an IGFBP-2 Polymorphism in the Irish Beef Herd', National Food Centre, Dublin, Royal Society of Chemistry Project Price

High School Diploma

Secondary College for Chemical Technology (HBLVA), Vienna, Austria, Specialization in Biochemistry, Biotechnology and Genetic Engineering, graduation with highest honors 07/2002
Diploma project: 'Study of A38 gene specifically expressed in totipotent tobacco microspores', Vienna Biocenter

Publications and Poster Presentation

Apprich S, Haas C, Höltinger S, Kneifel W, Novalin S, Schmid E, Siebenhandl-Ehn S; Vorstudie „Innovative Kleiebioraffinerie" CEREVAL; *BOKU Eigenverlag*; 01/2012

Schanda P, Haas C; Brutscher B, Konrat R, Tollinger M; Characterization of a folding intermediate of KIX using 15N/13C relaxation dispersion and fast 1H/2H amide exchange NMR spectroscopy; *XXIIIrd International Congress on Magnetic Resonance in Biological Systems*; San Diego; 08/2008

Singer CF, Gschwantler-Kaulich D, Fink-Retter A, Haas C, Hudelist G, Czerwenka K, Kubista E; Differential gene expression profile in breast cancer-derived stromal fibroblasts; *Breast Cancer Res Treat*. 2008 July; 110(2): 273-281

Hudelist G, Czerwenka K, Keckstein J, Haas C, Fink-Retter A, Gschwantler-Kaulich D, Kubista E, Singer CF; Expression of aromatase and estrogen sulfotransferase in eutopic and ectopic endometrium: evidence for unbalanced estradiol production in endometriosis; *Reprod Sci.* 2007 Dec;14(8):798-805